# Brain-sparing *sympathofacilitators* mitigate obesity without adverse cardiovascular effects

**Authors:** Inês Mahú[1], Andreia Barateiro[1,2], Eva Rial-Pensado[3], Noelia Martinéz-Sánchez[1], , Sandra H. Vaz[4,5], Pedro M. S. D. Cal[4], Benjamin Jenkins[6], Tiago Rodrigues,[4] Carlos Cordeiro[7], Miguel F. Costa[1,8], Raquel Mendes[1], Elsa Seixas[1,§], Mafalda M.A. Pereira[1,#], Nadiya Kubasova[1,$], Vitka Gres[1,†], Imogen Morris[1,‡], Carolina Temporão[1], Marta Olivares[9], Yolanda Sanz[9], Albert Koulman[6], Francisco Corzana[10], Ana M. Sebastião[4,5], Miguel López[3], Gonçalo J. L. Bernardes[4,11]*, Ana I Domingos[12]*

**Affiliations:**

[1]Obesity Laboratory, Instituto Gulbenkian de Ciência, Oeiras 2780-156, Portugal.
[2]Neuron Glia Biology in Health and Disease, Research Institute for Medicines (iMed.ULisboa), Faculty of Pharmacy, Universidade de Lisboa, Lisbon 1649-028, Portugal.
[3]NeurObesity Group, Department of Physiology, CIMUS, University of Santiago de Compostela–Instituto de Investigación Sanitaria, Santiago de Compostela (A Coruña) 15782, Spain.
[4]Instituto de Medicina Molecular João Lobo Antunes, Faculdade de Medicina, Universidade de Lisboa, Av. Prof. Egas Moniz, Lisbon 1649-028, Portugal.
[5]Instituto de Farmacologia e Neurociências, Faculdade de Medicina, Universidade de Lisboa, Av. Prof. Egas Moniz, Lisboa 1649-028, Portugal.
[6]NIHR BRC Core Metabolomics and Lipidomics Laboratory, Wellcome Trust-MRL Institute of Metabolic Science, University of Cambridge, Pathology building Level 4, Addenbrooke's Hospital, Cambridge CB2 0QQ, United Kingdom.
[7]Laboratório de FT-ICR e Espectrometria de Massa Estrutural, Faculdade de Ciências da Universidade de Lisboa, Lisbon 1749-016, Portugal.
[8]Department of Bioengineering, Instituto Superior Técnico, Universidade de Lisboa, Lisbon 1049-001, Portugal.
[9]Microbial Ecology, Nutrition & Health Research Unit. Institute of Agrochemistry and Food Technology, National Research Council, Valencia (IATA-CSIC), Catedratico Agustin Escardino 7, 46980, Paterna, Valencia, Spain.
[10]Departamento de Química, Universidad de La Rioja, Centro de Investigación en Síntesis Química, 26006 Logroño, Spain.
[11]Department of Chemistry, University of Cambridge, Lensfield Road, Cambridge CB2 1EW, UK.
[12]Department of Physiology, Anatomy and Genetics, University of Oxford, Parks Road, Oxford OX1 3PT, UK.

[§]Current address: Innate Immunity and Inflammation Laboratory, Instituto Gulbenkian de Ciência, Oeiras 2780-156, Portugal.
[#]Current address: Department of Neuronal Control of Metabolism, Max Planck Institute for Metabolism Research, Cologne 50931, Germany.
[$]Current address: DNA breaks Lab, Chronic Diseases Research Center (CEDOC), Universidade Nova de Lisboa, 1150-082 Lisbon, Portugal.
†Current address: Center for Chronic Immunodeficiency (CCI), Medical Center, Faculty of Medicine, University of Freiburg, 79106 Freiburg, Germany.
‡Current address: Center for Molecular Medicine, UMC Utrecht, Heidelberglaan 100, 3584 CX Utrecht, Holland.

***Correspondence:** A.I.D.: ana.domingos@dpag.ox.ac.uk; and G.J.L.B.: gb453@cam.ac.uk;

**Summary:**

Anti-obesity drugs in the amphetamine (AMPH) class act in the brain to reduce appetite and increase locomotion. They are also characterized by adverse cardiovascular effects with origin that, despite absence of any direct *in vivo* evidence, is empirically attributed to a peripheral sympathomimetic action in the heart. Here, we show that the cardiac side effects of AMPH originate in the brain and can be circumvented by PEGylation (PEGyAMPH) to exclude its central action. PEGyAMPH does not enter the brain and facilitates SNS activity via the $\beta_2$ adrenergic receptor, protecting mice against obesity by increasing lipolysis and thermogenesis, coupled to higher heat-dissipation which acts as an energy sink to increase energy expenditure without altering food intake or locomotor activity. Thus, we provide proof-of-principle for a novel class of exclusively peripheral anti-obesity *sympathofacilitators* that are devoid of cardiovascular and brain-related side effects.

**Keywords:**
obesity, sympathetic-nervous-system, *sympathofacilitators,* sympathomimetics, amphetamine, lipolysis, thermogenesis, heat-dissipation, thermoregulation

**Highlights:**

- PEGylated amphetamine (PEGyAMPH) is a first-in-class anti-obesity *sympathofacilitator,* acting via the $\beta_2$ adrenergic receptor.
- PEGyAMPH increases EE and weight loss, by coupling thermogenesis to heat-dissipation.
- PEGyAMPH does not enter the brain, nor has behavioural effects
- PEGyAMPH is cardioprotective, unless directly delivered into the brain

## Introduction:

Anti-obesity drugs in the amphetamine (AMPH) class, such as FDA-approved phentermine, are highly efficacious therapeutic compounds approved for common obesity (Cooke and Bloom, 2006; Melnikova and Wages, 2006). The potent anti-obesity effects of this class of drugs are reported to be mediated by a stimulant action in the brain that supresses appetite and promotes hyperkinesia (Cooke and Bloom, 2006; Heal et al., 2013; Melnikova and Wages, 2006). Although the anti-obesity effects of AMPH are unparalleled, these drugs are not only addictive, they also drive cardiovascular side effects such as tachycardia and hypertension. It is insofar unclear whether the cardiac side effects of AMPHs originate peripherally or centrally in the brain. Central action is a viable possibility, as the brain robustly controls heart rate and vascular capacitance in response to multiple internal and external stimuli (Malpas, 2010). However, despite the lack of direct experimental evidence, the peripheral model has prevailed wholly on empirical grounds.

Specifically, no direct evidence exists regarding the *in vivo* origin of cardiovascular side effects and whether a cardioneutral anti-obesity effect could result if AMPH is excluded from the brain.

All AMPHs are coined as *indirect sympathomimetics* because they block monoamine transporters thus increasing catecholamine availability (Cooke and Bloom, 2006; Heal et al., 2013; Melnikova and Wages, 2006). Recent evidence demonstrates that genetic loss-of-function of norepinephrine (NE) transporter (*Slc6a2*) outside the brain is sufficient for weight loss, without changes in food intake or locomotor activity (Pirzgalska et al., 2017). As such, we hypothesized that preventing access of AMPH to the brain would be sufficient to promote weight loss independently of behavior. To test this hypothesis, we chemically modified AMPH by PEGylation to increase its hydrodynamic radius and prevent its access to the brain (Pereira et al., 2017). PEGyAMPH does not cross the blood-brain barrier (BBB) yet retains the capacity to facilitate activation of sympathetic neurons and to increase peripheral NE availability in adipose tissues. This effect is mediated by the $\beta_2$ adrenergic receptor (ADRB2), a known mediator of vasodilation and smooth muscle relaxation (Chruscinski et al., 1999; Ernande et al., 2016). PEGyAMPH does not block Slc6a2, but it binds ADRB2, with preservation of residue interactions, in the same binding site as epinephrine. PEGyAMPH is devoid of cardiovascular effects, which emerge if directly delivered to the brain,. PEGyAMPH has an anti-obesity size effect similar to that of AMPH, yet without suppression of food intake or increased locomotion. Its anti-obesity effect is attributable to elevated lipolysis, lipid utilization and energy expenditure (EE), increased thermogenesis coupled to higher heat-dissipation, which contribute as an sink energy whilst overriding caloric intake (Jung et al., 1979; Kasza et al., 2019; Schwartz et al., 1983; Wang, 1924; Warner et al., 2013).

## Results

### 1. The anti-obesity effect of amphetamines requires an intact SNS.

Despite being classified as sympathomimetic, to our knowledge, there are no literature reports on the ability of AMPH to directly activate sympathetic neurons. To bridge this literature gap, we utilized electrophysiology and calcium imaging to probe the effects of AMPH on the excitability of sympathetic neurons isolated from superior cervical ganglia (SCG). We began by recording firing patterns of wild-type sympathetic neurons isolated from C57BL/6 mice (**Fig. 1. A-B**) by whole-cell patch-clamp recordings under current-clamp mode. We observed that AMPH significantly increases the maximum firing frequency (**Fig. 1. C**, left panel), although no significant changes in resting membrane potential were detected (**Fig. 1. C**, right panel). These results demonstrate that AMPH treatment increases the intrinsic excitability of peripheral sympathetic neurons. In parallel, we also used dissociated cultures of *TH-cre;*CAG-LSL-*GCaMP3* (GCaMP3$^+$) reporter mice to performe calcium imaging. Local application of acetylcholine (ACh), a physiologic pre-ganglionic activator, leads to an intracellular [$Ca^{2+}$] response in sympathetic neurons from GCaMP3$^+$ mice in control experiments, which results in significantly higher increases upon treatment with AMPH (**Fig. 1. D-F**).

Then, to investigate whether the increase of peripheral adrenergic signalling is required for the anti-obesity effect of AMPH, we subjected LSL-*DTR* (Control) and sympathectomized (**Sup. Fig. 1. A**) *TH-cre;* LSL-*DTR* mice (Symp mice - Pereira et al., 2017) to an obesogenic high fat diet

(HFD) accompanied with AMPH treatment [120 µmol/kg of body-weight (BW) or control phosphate-buffered saline (PBS), daily intraperitoneal (IP) injections] for a total of 6 weeks, and assessed BW-gain over time. As expected, AMPH treatment protects Control mice from diet-induced obesity (DIO; circular data points, **Fig. 1. G** and **Sup. Fig. 1B**). And, as we had previously reported (Pereira et al., 2017), Symp mice become extremely prone to DIO and gain twice as much weight as the Control group (white data points, **Fig. 1. G**). Surprisingly, both cohorts of Symp mice had very similar rate of BW-gain upon HFD exposure, regardless of treatment, which led to an approximately 40% increase after 6 weeks (triangular data points, **Fig. 1. G** and **Sup. Fig. 1. B**). This phenotype was independent of behavioural changes (**Fig. 1. H-J**), as upon treatment, both Control and Symp groups showed significant reduction in food intake (**Fig. 1. H**) and increase in locomotor activity (**Fig. 1. I-J**).

Hence, we theorized that, underlying this phenotype, was the reduction in peripheral sympathetic output (NE levels), which would cause depression of adrenergic-stimulated lipolysis (Caron et al., 2018; Pereira et al., 2017; Schwartz et al., 1983). To assess our hypothesis, we began by measuring the NE content in inguinal white adipose tissue (iWAT) of AMPH-treated mice and noted a significantly dampened response to AMPH treatment in Symp mice relative to Controls (**Fig. 1. K**). Additionally, we then analysed plasma lipid content to evaluate the levels of markers of lipolysis, which could explain the necessity of an intact SNS (**Sup. Fig. 1. C**). In fact, we found that in Symp mice, the behavioural effects of AMPH were not accompanied by an increase in SNS tone, nor by an elevation of lipolysis as seen in Control AMPH-treated mice (**Fig. 1. K** and **Sup. Fig. 1. C**).

Combined, these results strongly support that the sympathomimetic activity of AMPH is required for its protection against weight gain. More importantly, the reduced food intake and increased locomotion observed upon AMPH treatment are ineffective at reducing the rate of BW-gain in the absence of a functional SNS (Bray, 1991; Spraul et al., 1993)

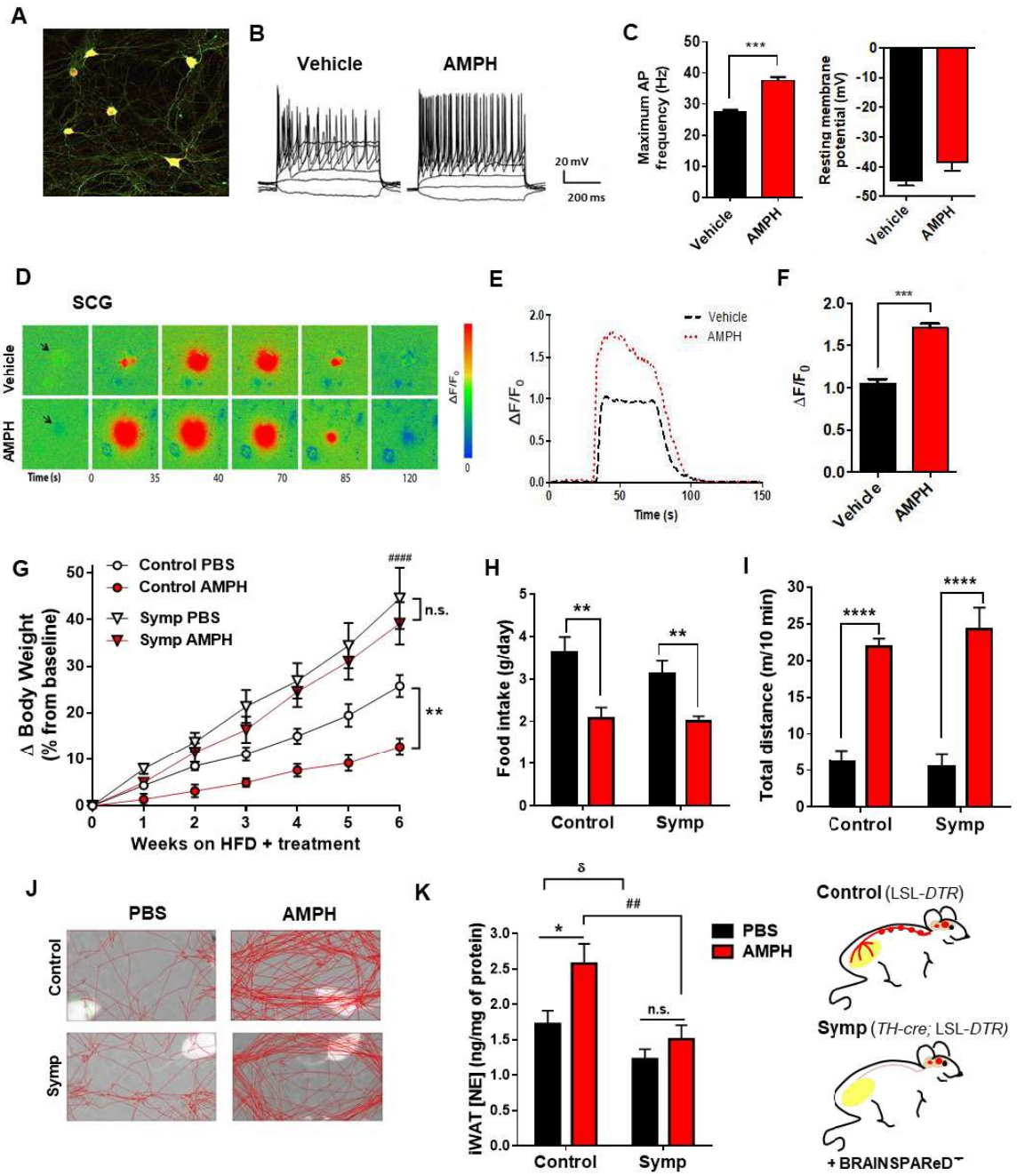


**Figure 1. Amphetamine (AMPH) facilitates SNS activation which is required for the anti-obesity effect, independently of hypophagia and hyperkinesia. A.** Cultured superior cervical ganglia (SCG) neurons transfected with Lenti-GFP and immuno-labelled for Tyrosine Hydroxylase (TH). **B.** Representative traces of changes in membrane potential and action potential (AP) evoked under current-clamp mode by injection 500ms current pulses (-25 to +275 pA in 25 pA increments) from an initial holding potential (Vh) of -70 mV in Vehicle and AMPH treatment. **C.** Maximum AP firing frequency of Vehicle and AMPH-treated neurons and Resting membrane potential of Vehicle and AMPH-treated neurons. **D.** Sequence of representative pseudocolor images showing calcium levels ($[Ca^{2+}]$) of one $GCaMP3^{+}$ SCG neuron after stimulation with 10 μM acetylcholine (ACh) for 40 s (arrow). In each frame, the timing after the onset of ACh

application is indicated. Changes in fluorescence (ΔF) were measured as relative elevation from baseline fluorescence and expressed as $\Delta F/F_0 = [(F_{post} - F_{rest})/F_{rest}]$ and are represented as pseudocolor scale. **E.** Representative ACh-induced [$Ca^{2+}$] elevation response tracings. **F.** Amplitude of ACh-induced $Ca^{2+}$ transients in Vehicle and AMPH-treated neurons (***p<0.001; n = 8; Statistics done using one-way ANOVA followed by Bonferroni correction). **G.** Change in Body Weight (ΔBW) of Control and regionally Sympathectomized (Symp) mice during 6 weeks of High Fat Diet (HFD) exposure plus treatment with Phosphate-Buffered Saline (PBS) or Amphetamine (AMPH) (dose: 120 µmol/kg of BW, daily IP injections). **H.** Daily food intake during HFD exposure and respective treatment. **I.** Representative tracking of the Locomotor activity of both Control and Symp mice, measured 1 h post injection. **J.** Total distance travelled in 10min, 1h post injection. **K.** Norepinephrine (NE) content in inguinal white adipose tissue (iWAT), of Control and Symp mice after 6 weeks of HFD exposure and treatment with PBS or AMPH (dose: 120 µmol/kg of BW, IP). (*p<0.05; **,##p<0.01; ***p<0.001; ****,####p<0.0001, n = 6-12. Statistics done using unpaired Student's *t*-test, with Holm-Sidak correction method. *PBS versus AMPH; δControl+PBS versus Symp+PBS, #Control+AMPH versus Symp+AMPH). Data presented as mean ± S.E.M. See also Figure S1.

## 2. PEGylation of AMPH prevents its access to the brain and its behavioural effects.

The BBB is generally impervious to large molecules, thus we resorted to chemical modification of AMPH by PEGylation (Pereira et al., 2017, see methods) to increase the hydrodynamic radius size, herein named PEGyAMPH (**Fig. 2. A**). To assess the success of this technique, we injected adult C57BL/6 mice with AMPH or PEGyAMPH (120µmol/kg of BW for both drugs or control PBS, IP) and collected brains 30 min and 2h afterwards. Brain extracts were then analysed by mass-spectrometry to detect the presence of either molecule (**Fig. 2. B**). The 30 min time-point was chosen for the analysis by the Fourier-transform ion cyclotron resonance (FT-ICR), because the half-life of AMPH in mice is reported to be 20 min (Riffee et al., 1978). Given its high resolution, one can identify the compound with errors lower than 1.5 ppm. From the replicate whole-brain samples, only in the group treated with AMPH was the drug detectable 30 min post-injection (**Fig. 2. B**). Additionally, we also processed brain tissue by liquid chromatography with mass-spectrometry LCMS detection (quantitative) and, possibly due to minimal penetration in areas where the BBB is not complete, we found a negligible quantity of PEGyAMPH relative to the levels observed of unmodified AMPH in the brain 30 min after IP administration, which then becomes undetectable 2h post-injection (**Fig. 2. C**). To confirm the brain mass-spectrometry analysis and consolidate our *in vivo* results, we also probed behavioural alterations in mice after IP administration of both drugs (**Fig. 2. D-F**). According to our previous results, AMPH treatment consistently supresses food intake (**Fig. 2. D**) and increases locomotor activity in mice (**Fig 2. E** and **F**). Importantly, we did not observe any changes in feeding behavior (**Fig. 2. C**) nor locomotion (**Fig. 2. D** and **E**) in PEGyAMPH-injected mice relative to those of the control PBS-treated animals.

Thus, we could conclude that PEGylation of AMPH (PEGyAMPH) successfully restrains its brain penetrance.

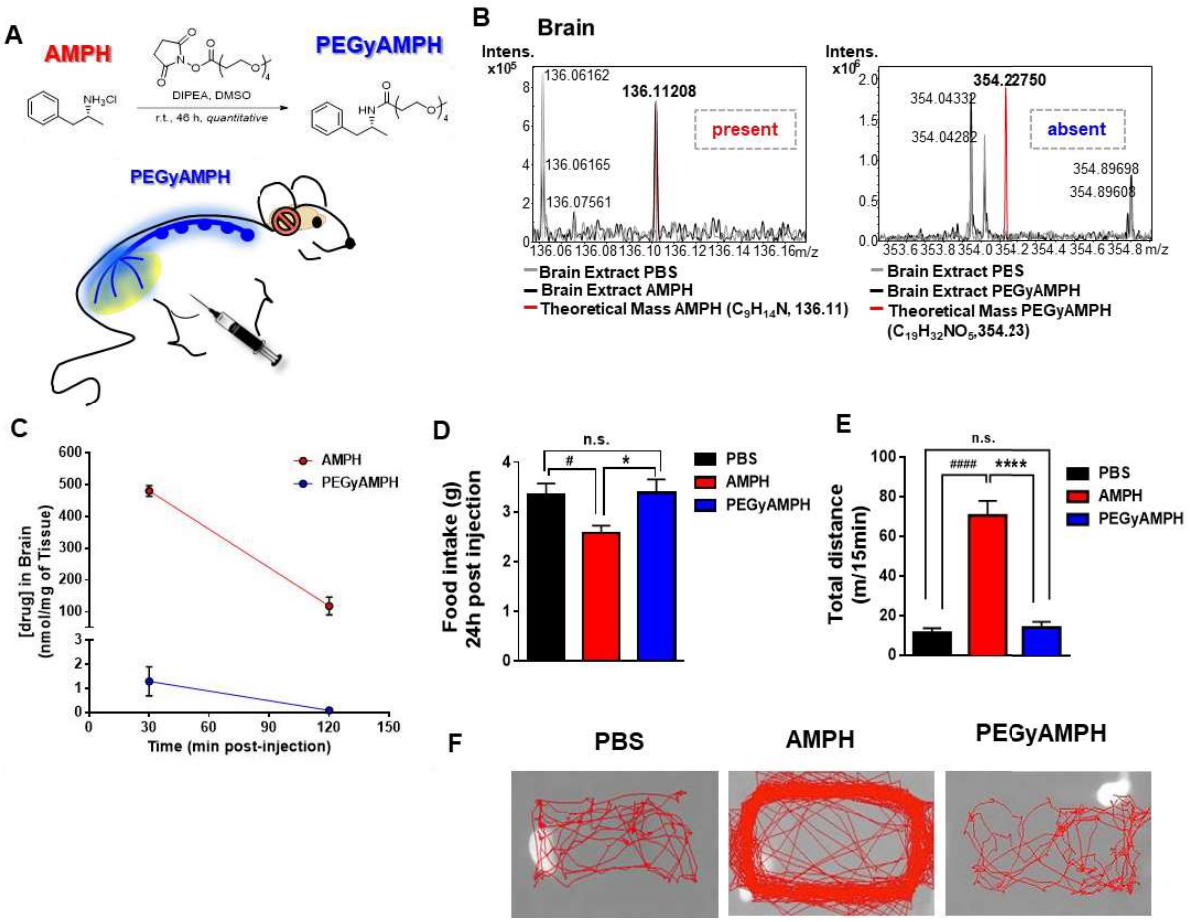


**Figure 2. PEGylated Amphetamine (PEGyAMPH) does not enter the brain and does not induce hypophagia nor hyperkinesia. A.** Representative scheme of the AMPH's PEGylation method to produce PEGyAMPH. **B.** Representative Fourier-transform ion cyclotron resonance (FT-ICR) mass spectra of brain extracts from C57BL/6 mice 30 min post-injection with PBS, AMPH or PEGyAMPH (dose: 120 µmol/kg of BW for both drugs, IP). **C.** Brain levels of AMPH and PEGyAMPH after IP injection. **D.** 24h food intake post-injection with PBS, AMPH or PEGyAMPH (normal diet) **E.** Total distance travelled in 15min **F.** Representative tracking of locomotor activity, measured 1 h post-injection. (*,$^{\#}$p<0.05; ****,$^{\#\#\#\#}$p<0.0001, n = 4-10. Statistics done using unpaired Student's *t*-test, with Holm-Sidak correction method*PBS versus PEGyAMPH; $^{\#}$PBS versus AMPH.) Data presented as mean ± S.E.M. See also Figure S2.

### 3. PEGyAMPH facilitates SNS activation, via $\beta_2$-adrenoceptor (ADRB2) signaling.

Next to investigate PEGyAMPH's biologic activity, we treated SCG neurons with either AMPH or PEGyAMPH and recorded the firing patterns, using whole-cell patch-clamp recordings under current-clamp mode (**Fig. 3. A-B and Sup. Fig. 3. A-C**). The maximum firing frequency of PEGyAMPH-treated neurons significantly increased relative to the control (**Fig. 3. B**), like AMPH, with no significant changes in resting membrane potential (**Sup. Fig. 3. A**). There was also a significant increase in action potential (AP) firing threshold only detected between Vehicle and PEGyAMPH-treated neurons (**Sup. Fig. 3. B**) and in the Δ depolarization for AP firing (**Sup. Fig. 3. C**). These results confirm that PEGyAMPH has an identical effect as AMPH, namely it increases

the intrinsic excitability of sympathetic neurons. Additionally, we also assessed the effects of PEGyAMPH on free intracellular [$Ca^{2+}$] levels of sympathetic neurons isolated from GCaMP3$^{+}$ mice. There was a significant increase of ACh-induced calcium responses ($\Delta F/F_0$) after incubation with PEGyAMPH, relative to control values, similar to that observed in AMPH-treated sympathetic neurons (**Fig. 3. C-E**). To further confirm whether PEGyAMPH, like AMPH, had the capacity to elevate peripheral sympathetic tone, we conducted a dose response curve probing the NE content in iWAT and the livers of adult C57BL/6 male mice (**Fig. 3. E**). As expected, we found that PEGyAMPH increases NE content in metabolic tissues in a dose-dependent manner (**Fig. 3. E**). Moreover, to try to explain the biologic effect of PEGyAMPH, we also probed the effects of PEGylation on the drug's pharmacologic properties. Pharmacokinetic analysis of both drugs revealed that PEGyAMPH has shorter circulating half-life compared to that AMPH (**Sup. Fig. 2. A**, 0.2 h vs 0.36 h, respectively), while it also appears to be more quickly metabolized in the liver (**Sup. Fig. 2. B**). As expect, the PEGylation greatly reduced the drug's excretion by the urine (**Sup. Fig. 2. C**) (Harris and Chess, 2003). To explore the functional properties of PEGyAMPH, we began by assessing its capacity to bind to the NE transporter (Slc6a2) *in vitro*, as this is reported to be a major target of AMPH (Heal et al., 2013). Of note, we observed a marked difference in capacity for binding Slc6a2; as AMPH displaces ~80% of the radioligand at 50 μM, while its PEGylated counterpart shows no activity at the same concentration (**Sup. Fig. 2. D**). This suggests that PEGyAMPH's pharmacology differs from that of its unmodified counterpart.

As such, we next evaluated the effect of replacing the $NH_3^+$ by an amide group in potential interactions of PEGyAMPH with adrenoceptors that have available X-ray structures. For this, we started by conducting docking calculations for both AMPH and PEGyAMPH with either the $\beta_1$-adrenoceptor (ADRB1) or the $\beta_2$-adrenoceptor (ADRB2) (**Sup. Fig. 3. D** and **Fig. 3. F**, respectively**)**. The X-ray structure reported for these receptors in complex with epinephrine (pdb ID: 6H7J and 4LDO, respectively) (Ring et al., 2013) was used as a 3D model of the protein. Of note, we found that both compounds occupy the same binding site as epinephrine. And these rigid-docking structures were also minimized in explicit solvent and ions using AMBER and GAFF force fields (Maier et al., 2015; Wang et al., 2004). According to our calculations, we found that the $NH_3^+$ group of AMPH is engaged in a hydrogen bond with the side chain of Asp256 of the ADRB2 (**Fig. 3. F**, left panel, see Methods for details). In addition, the methyl group of the drug is involved in a CH/π interaction with Phe336 of this receptor, and its aromatic ring establishes hydrophobic contacts with several residues of ADRB2. Importantly, the complex between PEGyAMPH and ADRB2 is also stabilized by several hydrogen bonds. In particular, a prevalent hydrogen bond between the NH group of PEGyAMPH is formed with the side chain of Asp256 of the receptor, and an additional one involves the carbonyl group of this PEGylated compound and Tyr423 of ADBR2. Furthermore, the PEG chain of the drug is involved in two other hydrogen bonds with the side chains of His236 and Lys240 of ADRB2 (**Fig. 3. F**, right panel).

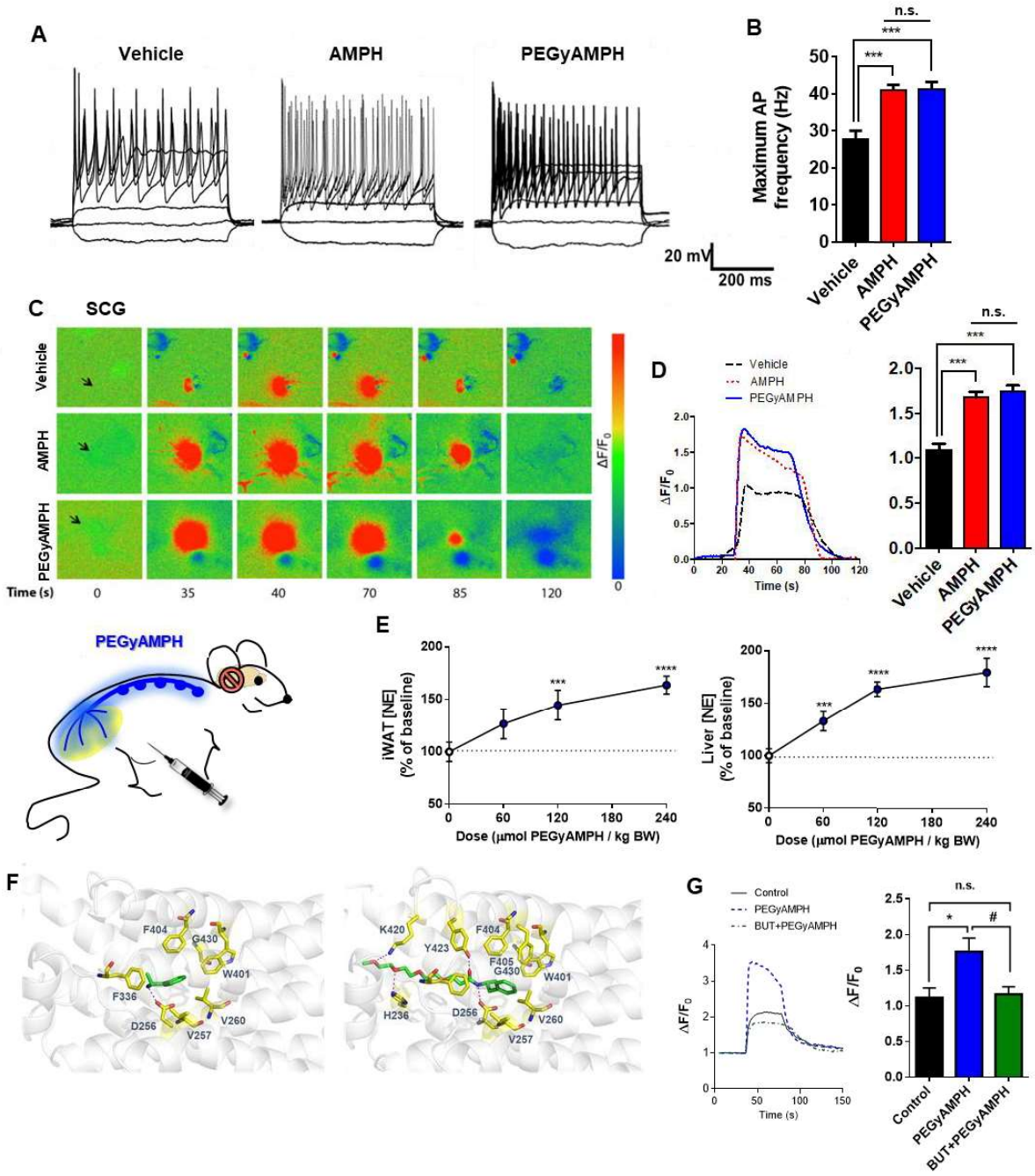


**Figure 3. PEGyAMPH facilitates SNS activation, via $\beta_2$-adrenoceptor (ADRB2) signaling. A.** Representative traces of changes in membrane potential and action potential (AP) evoked under current-clamp mode by injection 500-ms current pulses (-25 to +275 pA in 25 pA increments) from an initial holding potential (Vh) of -70 mV in Vehicle, AMPH and PEGyAMPH treatment. **B.** Maximum AP firing frequency of Vehicle, AMPH and PEGyAMPH-treated neurons. **C.** Sequence of representative pseudocolor images showing $[Ca^{2+}]_i$ changes of one GCaMP3$^+$ superior cervical ganglia neuron after stimulation with 10 µM ACh for 40 s (arrow). In each frame, the timing after the onset of ACh application is indicated. Changes in fluorescence (ΔF) were measured as relative elevation from baseline fluorescence and expressed as $\Delta F/F_0 = [(F_{post} - F_{rest})/F_{rest}]$ and are represented as pseudocolor scale. **D.** Representative ACh-induced $[Ca^{2+}]_i$

elevation response tracings in Vehicle, AMPH and PEGyAMPH-treated neurons (left), and Amplitude of ACh-induced $Ca^{2+}$ transients in Vehicle-treated neurons and after pharmacological treatment with AMPH and PEGyAMPH (right). (***p<0.001; n = 3-4; Statistics done using one-way ANOVA followed by Bonferroni correction). **E.** Increase in NE content of iWAT (left) and liver (right) of C57BL/6 mice 3h post-treatment with PEGyAMPH (doses: 60, 120 or 240 µmol/kg of BW,IP injections) without access to food, relative to baseline levels. **F.** 3D structure of $\beta_2$-adrenoceptor in complex with AMPH and PEGyAMP. Left: Minimized structure calculated by Molecular Mechanics (MM) for ADRB2/AMPH complex, showing the most relevant interactions between AMP and the receptor. Right: Minimized structure calculated by MM for ADRB2/PEGyAMPH complex, showing the most relevant interactions ligand-receptor. ADBR2 is represented as white ribbons and the carbon atoms of the residues of this receptor that are interacting with the ligands are in yellow. The carbon atoms of the ligands are in green. **G.** Representative ACh-induced $[Ca^{2+}]_i$ elevation response (left), and amplitude of ACh-induced $Ca^{2+}$ transients in Vehicle-treated neurons and after pharmacological treatment with PEGyAMPH, in the absence and presence of the ADRB2 antagonist butoxamine (BUT) (right). (***p<0.001; n = 3-4; Statistics done using one-way ANOVA followed by Bonferroni correction). (*,$^{\#}$p<0.05; ***p<0.001; ****p<0.0001, n = 8-12. Statistics done using unpaired Student's *t*-test, with Holm-Sidak correction method. *PBS versus PEGyAMPH; $^{\#}$PEGyAMPH versus PEGyAMPH+BUT) Data presented as mean ± S.E.M. See also Figure S3.

As reported by our calculations, the replacement of the $NH_3^+$ by an amide group does not significantly disturb the interactions with the adrenoceptors tested (**Fig. 3. F** and **Sup. Fig. 3. D**, ADRB1 and ADRB2, respectively). This aligns with the ability of PEGyAMPH to modulate sympathetic tone to metabolic tissues (**Fig. 3 E** and **Sup. Fig. 3 E-F**). Moreover, to experimentally probe the effect of specific engagement of ADRB2 by PEGyAMPH on its *sympathofacilitator* properties, we performed ACh-induced $[Ca^{2+}]$ elevation response imaging assays and found that butoxamine (BUT - a selective ADRB2 antagonist; Gabanyi et al., 2016) blocked PEGyAMPH's capacity to amplify neuronal activation by ACh (**Fig. 3. G**).
Hence, PEGylation of AMPH changed its pharmacology, but it did not reduce the *sympathofacilitator* activity, which seems to rely on ADRB2 engagement.

### 4. PEGyAMPH does not affect cardiovascular function in mice, unless it is centrally delivered.

The anti-obesity effects of AMPH-like compounds are proposed to be driven by its modulation of behaviour, yet these drugs are coined *sympathomimetics* (Heal et al., 2013) in reference to their well-known cardiovascular side effects, such as tachycardia and hypertension. Surprisingly, we found that the respiratory and cardiovascular effects characteristic of AMPH were absent when PEGyAMPH is administered intraperitoneally (**Fig. 4. A-C,** and **Sup. Fig. 4. A**). In fact, it is insofar unclear whether the cardiac sympathomimetic effects of AMPHs originate peripherally, by direct activation of the SNS, or centrally, by brain-dependent action (Heal et al., 2013). Surprisingly, although *sympathomimetic* drugs are classically described to exert excitatory effects on the cardiovascular system, our peripherally acting drug did not cause elevation of blood pressure (**Fig. 4. A** and **B**) or heart rate (**Fig. 4. C** and **Sup. Fig. 4. A**, right panel). Concomitantly, we also detected less accumulation of the drug (**Sup. Fig. 4. B**) and of NE in the hearts (**Sup. Fig. 4. C**) of animals treated with PEGyAMPH compared to those of treated with AMPH via IP.

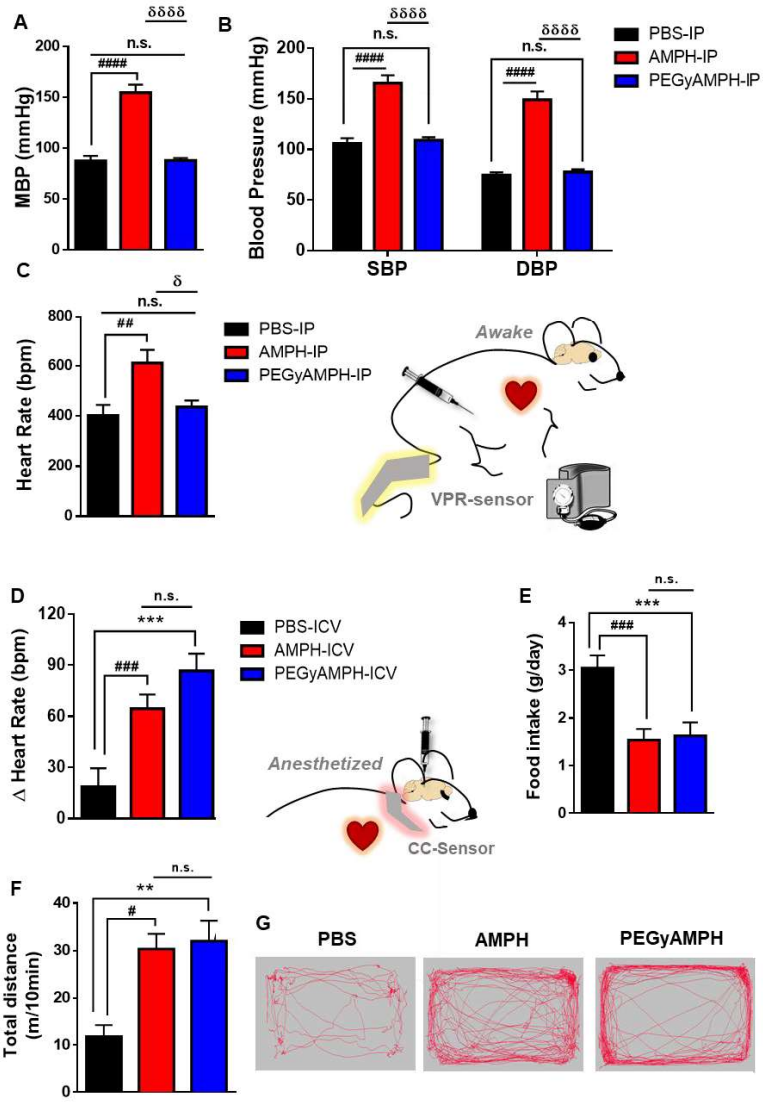


**Figure 4. PEGyAMPH, unlike AMPH, does not affect cardiovascular function, unless delivered centrally.** **A.** Mean Blood Pressure (MBP) **B.** Systolic Blood Pressure (SBP) and Diastolic Blood Pressure (DBP) **C.** Heart rate of C57BL/6 mice, recorded 30-45 min post-injection with PBS, AMPH or PEGyAMPH (dose: 120 µmol/kg of BW for both drugs, IP) using a non-invasive Volume Pressure Recording (VPR) tail-cuff system (**D-G**) Measurements taken post-ICV injection of PBS, AMPH or PEGyAMPH (60nmol, bolus, per animal) **D.** Change in heart rate recorded 15 min post-injection under anesthesia (2% isoflurane) using a CollarClip Sensor (CC-Sensor) for pulse-oximetry. **E.** 24h food intake of ICV-injected mice **F.** Total distance travelled in 10 min **G.** Representative tracking of locomotor activity, recorded 15-30 min post-injection. ($^{\#,\delta}p<0.05$; $^{**,\#\#}p<0.01$; $^{***,\#\#\#}p<0.001$; $^{\#\#\#\#,\delta\delta\delta\delta}p<0.0001$, n = 8-12. Statistics done using unpaired Student's *t*-test, with Holm-Sidak correction method. *PBS versus PEGyAMPH; $^{\#}$PBS versus AMPH, $^{\delta}$PEGyAMPH versus AMPH) Data presented as mean ± S.E.M. See also Figure S4.

A central action seems to be a viable possibility, as the brain robustly controls heart rate and vascular capacitance in response to multiple internal and external stimuli (Malpas, 2010). To test this hypothesis, we probed the effect of central administration of both drugs via intracerebroventricular (ICV) injection (bolus of 60nmol, for PEGyAMPH or AMPH). As expected, PEGyAMPH had equivalent anorexic effect (**Fig. 4. E**) and capacity to induce hyperkinesia (**Fig. 4. F-G**) as AMPH. Importantly, we confirmed that ICV injections were sufficient to induce excitatory effects on the cardiorespiratory system (**Fig. 4. D** and **Sup. Fig. 4. D**).

Combined, our results suggest that the well-described cardiovascular stress induced by *sympathomimetic* drugs is driven by their central action on the brain.

## 5. PEGyAMPH protects mice from obesity by elevating EE, without affecting feeding behaviour or locomotor activity.

Recent evidence from our group and others (Camell et al., 2017; Pereira et al., 2017; Pirzgalska et al., 2017) clearly demonstrates that peripheral NE regulates adiposity levels independent of food intake or exercise. As such, we hypothesized that PEGyAMPH treatment would be sufficient to promote long term anti-obesity results regardless of excess caloric intake. To investigate this, we exposed adult C57BL/6 mice to HFD and treatment with either AMPH or PEGyAMPH (120 µmol/kg of BW for both drugs or control PBS, daily IP injections) for a total of 10 weeks and subsequently assessed their rate of weight gain and metabolic alterations. As demonstrated before, AMPH therapy protects wild type mice from DIO after 10 weeks of HFD (**Fig. 5. A** and **B**, red data points). Moreover, PEGyAMPH's *sympathofacilitator* activity is sufficient to protect BW in dose-dependent manner (**Sup. Fig. 3. G**). Notably, when administrated in equimolar dose, treatment with PEGyAMPH showed similar size effect on promoting leanness under HFD exposure to that of its unmodified counterpart. (**Fig. 5. A** and **B**, blue data points). Both therapies improved peripheral insulin sensitivity, as blood glucose levels did not differ between all the HFD-exposed groups (**Sup. Fig. 5. A**), but the circulating plasma insulin levels were significantly lower in the treated groups compared to those of PBS controls (**Sup. Fig. 5. B**)**.** Given that the SNS is reported to not only control insulin sensitivity but also insulin secretion (Morton et al., 2017, Nonogaki, 2000; Ruud et al., 2017), we quantified the NE content in the pancreas of C57BL/6 mice after 10 weeks of HFD exposure and respective treatment, and observed that only AMPH increased SNS output to this tissue (**Sup. Fig. 5. C**). Thus, PEGyAMPH treatment prevents the development of hyperinsulinemia and improves glucose homeostasis by increasing peripheral insulin sensitivity without suppressing its secretion. Of note, analysis of liver gene expression revealed that both treated groups had a two-fold elevation of phosphoenolpyruvate carboxykinase (*PEPCK*) gene expression (**Sup. Fig. 5. D**), which is a major integrator of energy metabolism (Burgess et al., 2007; Petersen et al., 2017; She et al., 2000). The higher insulin sensitivity found in treated animals during the fed-state was not associated with significant differences in glucose levels during an IP glucose tolerance test (GTT - **Sup. Fig. 5. E** and **G**). Yet, the PEGyAMPH-treated group revealed a trend towards higher peripheral glucose uptake during an insulin tolerance test (ITT - **Sup. Fig. 5. F** and **H**). Combined, these results indicate that long-term treatment with PEGyAMPH protects mice from DIO and improves glucose homeostasis during HFD exposure. As expected, we found that PEGyAMPH-treated mice did not decrease their food intake (**Fig. 5. C**) nor increase locomotor activity (**Fig. 5. D** and **Sup. Fig. 5. H**) upon chronic treatment. Nonetheless, indirect calorimetry revealed that, under HFD feeding, this group had slightly higher EE compared to the PBS controls (**Fig. 5. E.** and **Sup. Fig. 5. G**) despite having similar behaviour.

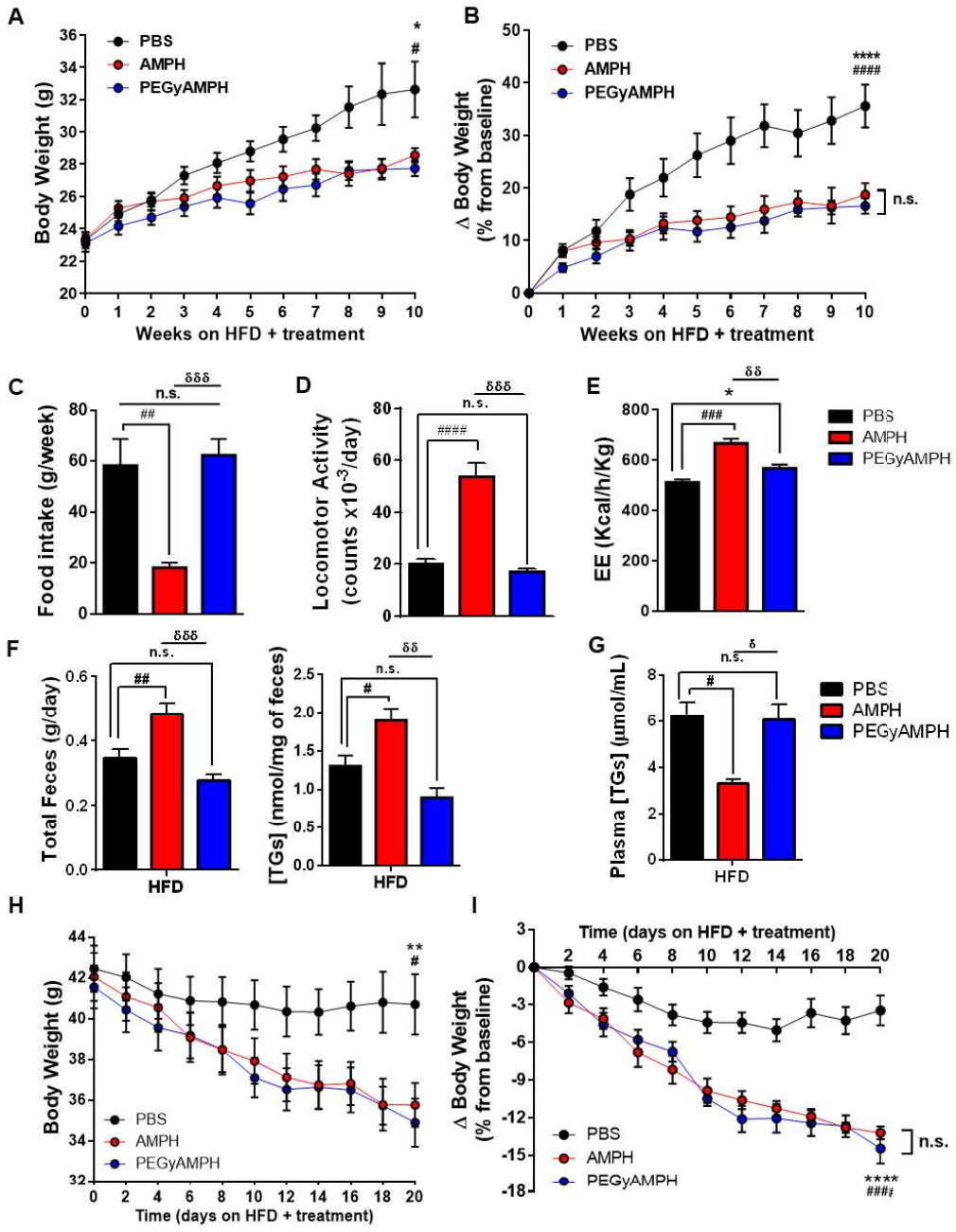


**Figure 5. PEGyAMPH protects mice from diet-induced obesity (DIO) and increases energy expenditure (EE) without affecting food intake. A.** Body weight and **B.** change in body weight (ΔBW) of C57BL/6 mice during 10 weeks of HFD exposure with PBS, AMPH or PEGyAMPH treatment (dose: 120 μmol/kg of BW for both drugs, daily IP injections) **C.** Weekly food intake of HFD **D.** Quantification of daily locomotor activity in beam break counts per day **E.** Total 48h normalized EE **E.** Daily fecal output (left) and fecal TGs content (right) **G.** Plasma TGs levels measured 2h post-injection without access to food **H.** Body weight and **I.** ΔBW of diet induced obese (DIO) mice during 3 weeks of treatment with PBS, AMPH or PEGyAMPH (dose: 120 μmol/kg of BW for both drugs, daily IP injections). (*,$^{\#}$,$^{\delta\delta}$p<0.05; **,$^{\#\#}$,$^{\delta\delta}$p<0.01; $^{\#\#\#}$,$^{\delta\delta\delta}$p<0.001; ****,$^{\#\#\#\#}$p<0.0001, n = 8-15. Statistics done using unpaired Student's *t*-test, with Holm-Sidak correction method. *PBS versus PEGyAMPH; $^{\#}$PBS versus AMPH; $^{\delta}$PEGyAMPH versus AMPH.) Data presented as mean ± S.E.M. See also Figure S5.

Moreover, we also analysed the effects of PEGyAMPH treatment on dietary lipid absorption and found that PEGyAMPH did not alter the total 24h fecal output nor its lipid content (**Fig. 5. F**). Concomitantly, plasma TGs levels of PEGyAMPH-treated mice were also unchanged relative to controls (**Fig. 5. G**). Hence, we can conclude that PEGyAMPH promotes leanness by overriding caloric intake during HFD exposure. Finally, to test the efficacy of the treatments in inducing weight loss in already-obese animals, we also treated C57BL/6 mice previously exposed for minimum of 3 months to HFD with either AMPH or PEGyAMPH (120 µmol/kg of BW, IP), and found that both drugs caused significant weight loss (>10%) after just 3 weeks of daily injections (**Fig. 5. H-I**). Altogether, our results suggest that treatment with PEGyAMPH during HFD exposure overrides food intake by increasing EE and adrenergic-stimulated metabolic pathways.

### 6. PEGyAMPH protects from obesity by elevating lipolysis and lipid utilization.

Given that PEGyAMPH's metabolic effects during DIO are dose dependent, as are its *sympathofacillitor* properies (**Sup. Fig. 3. G** and **Fig. 3. E**, respectively), to begin dissecting the anti-obesity mechanism we started by analysing the sympathetic output to adipose tissue of C57BL/6 mice after 10 weeks of HFD exposure and chronic treatment. Surprisingly, the PEGyAMPH-treated group exhibited a significantly greater increase in NE content in iWAT compared not only to the control group but also with that of the AMPH-treated animals (**Fig. 6. A**). This was also associated with the presence of much higher levels of lipolytic markers in circulation, namely free fatty acids (FFAs **– Fig. 6. B**) and glycerol (**Fig. 6. C**), highlighting the potential of PEGyAMPH for chronic treatment. Nonetheless, we observed a marked reduction in iWAT adipocyte size (**Fig. 6. D** and **E**) in both treated groups relative to the same depot of PBS-treated animals after HFD exposure.

Next, we probed changes in gene expression of metabolic tissues induced by both treatments. PEGyAMPH induced an almost three-fold increase $\beta_3$ adrenergic receptor (*ADRB3*) expression in WAT, but not in BAT, after 10 weeks of HFD exposure (**Fig. 6. F** and **G**). We also evaluated the levels of other lipolysis-associated genes after treatment and observed that PEGyAMPH induced a two-fold upregulation of hormone-sensitive lipase (*HSL*) in both WAT and BAT, whereas adipose triglyceride lipase (*AtgL*) was only elevated in WAT (**Fig. 6. F** and **G**). Combined with the upregulation of adipose lipolysis, SNS output was also elevated in liver (**Sup. Fig. 6. A**) and skeletal muscle (**Sup. Fig. 6. D**) after treatment with PEGyAMPH during HFD feeding, which suggests higher metabolic performance, *i.e.* higher utilization of lipid stores (Geerling et al., 2014; Nonogaki, 2000). In line with this hypothesis, we found decreased TG content (**Sup. Fig. 6. B**), accompanied by an increase of glycogen (**Sup. Fig. 6. C**) in the livers of PEGyAMPH-treated mice. By performing Oil-Red O (ORO) staining and quantification (**Fig. 6. H** and **I**), we confirmed a marked reduction in hepatic steatosis. In the skeletal muscle of these animals, PEGyAMPH caused a reduction in the levels of TGs (**Sup. Fig. 6. E**) while preserving glycogen stores (**Sup. Fig. 6. F**). Quantification of gene expression in the liver and muscle also revealed alteration of lipid metabolism in these tissues (**Sup. Fig. 6. G** and **H**, respectively).

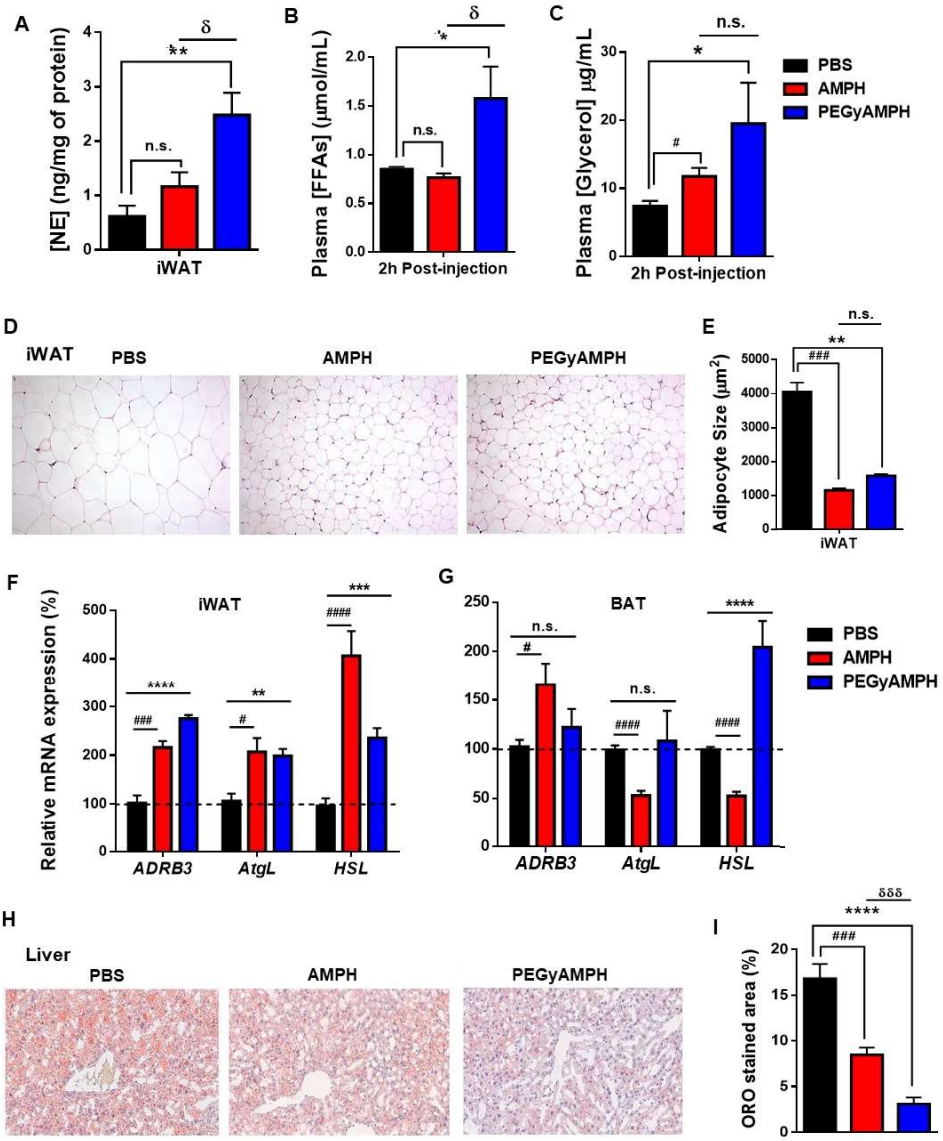


436

437 **Figure 6. PEGyAMPH elevates adipose tissue lipolysis and peripheral lipid utilization during DIO. A.**
438 NE content in iWAT of C57BL/6 mice after 10 weeks of HFD exposure and treatment with PBS, AMPH or
439 PEGyAMPH (dose: 120 µmol/kg of BW for both drugs, daily IP injections) **B** and **C.** Plasma levels of FFAs
440 (**B**) and glycerol (**C**) of C57BL/6 mice 2 h post-injection with PBS, AMPH or PEGyAMPH without access to
441 food, measured 4-5 weeks after the start of HFD exposure and respective treatment **(D-I)** Histology and
442 gene expression analysis of metabolic tissues from C57BL/6 mice after the conclusion of 10 weeks of HFD
443 exposure and treatment with PBS, AMPH or PEGyAMPH. **D.** Representative histologic slices of iWAT
444 stained with haematoxylin and eosin (H&E) and **E.** Quantification of iWAT adipocyte size **F** and **G.** Lipolytic
445 gene expression levels of $\beta_3$ adrenergic receptor (*ADRB3*), Adipose triglyceride lipase (*AtgL*) and Hormone-
446 sensitive lipase (*HSL*) in iWAT (**F**) and in BAT (**G**) determined by qRT-PCR relative to housekeeping gene
447 *Arbp0* **H.** Representative histologic slices of liver with Oil-Red O (ORO) staining **I.** ORO-stained liver area
448 normalized to the total area. (*,$^{\#}$,$^{\delta}$p<0.05; **p<0.01; ***,$^{\#\#\#}$,$^{\delta\delta\delta}$p<0.001; ****,$^{\#\#\#\#}$p<0.0001, n = 5-12. Statistics
449 done using unpaired Student's *t*-test, with Holm-Sidak correction. *PBS versus PEGyAMPH; $^{\#}$PBS versus
450 AMPH; $^{\delta}$PEGyAMPH versus AMPH.). Data presented as mean ± S.E.M. See also Figure S6.

Hence, our results indicate that PEGyAMPH's protection against DIO is associated with a general elevation of peripheral lipid breakdown and utilization, highlighting the SNS as a major regulator of adiposity during excessive caloric intake.

### 7. PEGyAMPH protects from obesity by elevating thermogenesis and heat dissipation via ADR2B.

Activation of thermogenesis, which is also controlled by the SNS and can act as an *energy sink,* is proposed to promote resistance to obesity (Rothwell and Stock, 1979). Nonetheless, the rapid increase in EE observed upon AMPH administration could be a result of increased locomotor activity, and thus the contribution of its thermogenic activity to the elevation of basal metabolic rate and BW management is still debated (Arch and Trayhurn, 2013). To probe the thermogenic effect of each drug, we began by using thermographic photography to analyse BAT temperature in HFD-fed mice. After PEGyAMPH treatment, there was an elevation in BAT temperature similar to that evoked by AMPH (2h post-injection - **Fig. 7. A** and **B**). Accordingly, we also found that after 10 weeks of HFD and drug treatment, both amphetamines caused a fifteen-fold upregulation of the primary BAT thermogenic marker, uncoupling protein 1 (*UCP1*), and increased all other thermogenic genes probed (**Fig. 7. C**). This was accompanied by an eight-fold increase in the levels of expression of glucose-transporter-type-4 isoform (*GLUT4)* in BAT of mice treated with both drugs (**Sup. Fig. 7. A**), which indicates higher glucose uptake by this organ. GLUT4 has been reported to be a marker for higher thermogenic activity (Lee et al., 2016) and could account for the increased insulin sensitivity compared to PBS-treated controls (**Sup. Fig. 5. B**). Although *UCP1* levels were not changed in iWAT, the other thermogenic genes quantified were upregulated relative to the levels observed in the control group (**Sup. Fig. 7. A**), and others have reported thermogenesis with invariant UCP1 (Granneman et al., 2003; Ikeda et al., 2017, 2018). The combination of these results points to a general trend for elevated thermogenesis after PEGyAMPH treatment, which underlies its protection against DIO, overriding caloric intake.

Surprisingly, we also detected that only AMPH caused transient hyperthermia after its administration (Borbély et al., 1974), while PEGyAMPH-treated mice remain normothermic, i.e. they had core body temperature identical to that of the control group (**Fig. 7. D**). This suggests that, although both drugs act as sympathomimetics, they might actually have different actions on peripheral heat dissipation (Blessing et al., 2016). Hence, to assess vasoconstriction at the extremities, we probed the local temperature at the tail base by thermography (Fischer et al., 2016, Warner et al., 2013). As such, we found that, despite the similar core body temperature, PEGyAMPH-injected mice had significantly warmer tails relative to those of the PBS controls (**Fig. 7. E** and **F**). This indicates that, unlike AMPH, PEGyAMPH's sympathomimetic activity increases thermogenesis without causing vasoconstriction, suggesting that heat dissipation could be a relevant component of body weight regulation (Jéquier et al., 1974; Kasza et al., 2019; Warner et al., 2013). Given that PEGyAMPH-treated mice seem to rely on activation of thermogenesis to remain lean, we also probed the effect of the drug during HFD exposure under thermoneutral housing conditions. As expected, PEGyAMPH weight-reducing potency is decreased in this environmental setting, yet some level of protection against DIO does remain (**Fig. 7. G** and **Sup. Fig. 7 E**).

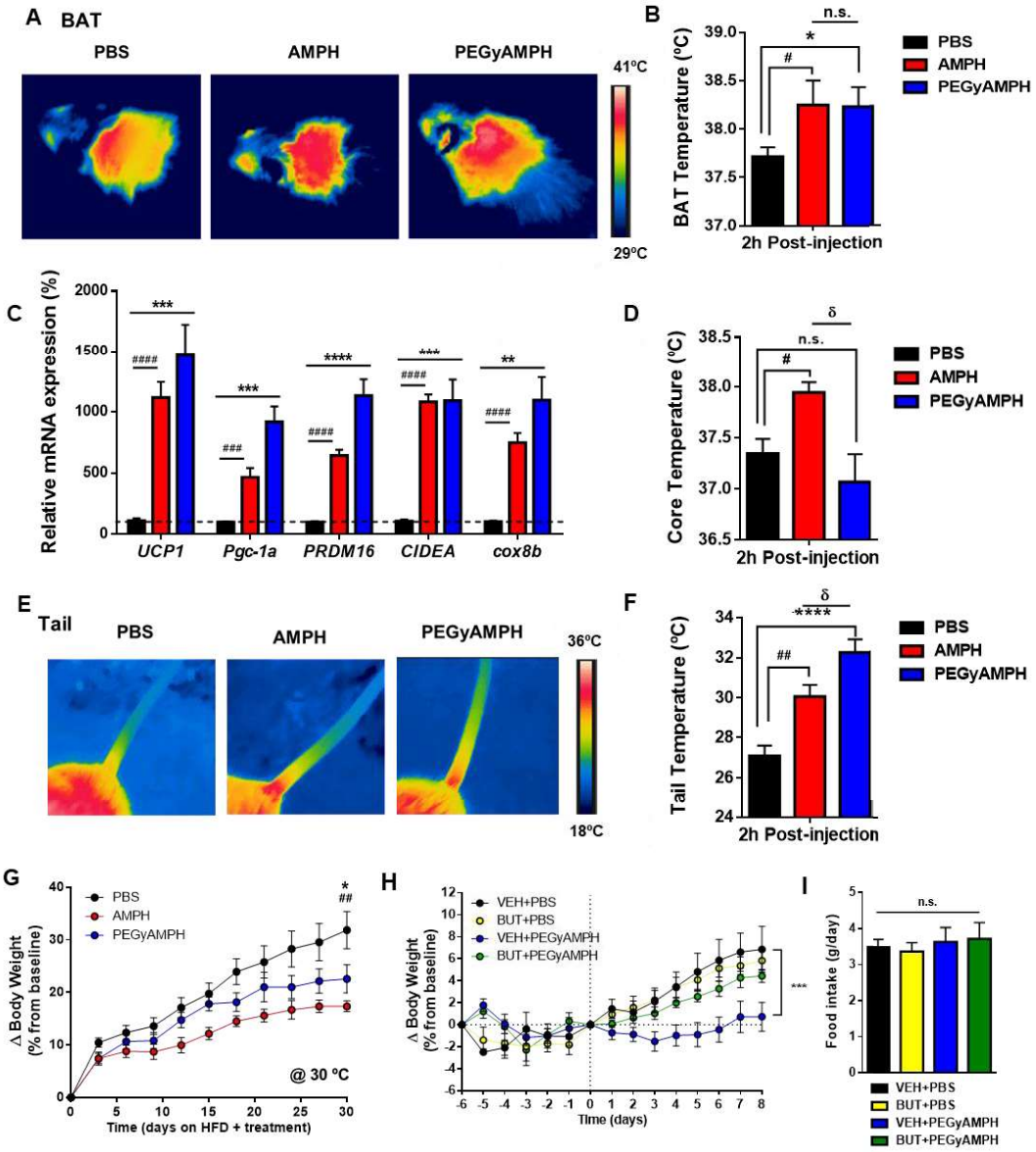


**Figure 7. PEGyAMPH increases thermogenesis, heat dissipation and protects against obesity via ADR2B.** All thermal measurements were performed 2 h post-injection with PBS, AMPH or PEGyAMPH (dose: 120 µmol/kg of BW for both drugs, IP. **A.** Representative infrared thermography of the BAT area temperature **B.** Quantification of BAT skin area temperature measured with thermography **C.** BAT mRNA levels of thermogenic genes determined by qRT-PCR relative to housekeeping gene *Arbp0*, after 10 weeks of HFD exposure and treatment with PBS, AMPH or PEGyAMPH **D.** Core body temperature measured with rectal probe **E.** Representative infrared thermography of tail temperatures. **F.** Quantification of tail temperature measured 0,5 cm from the tail base with thermography **G.** ΔBW of C57BL/6 mice mice exposed to HFD and treatment with PBS, AMPH or PEGyAMPH (dose: 120 µmol/kg of BW for both drugs, daily IP injections) under thermoneutral housing conditions **H.** ΔBW and **I.** Daily food intake of C57BL/6 mice exposed to HFD and treatment with PBS or PEGyAMPH (dose: 120 µmol/kg of BW, daily IP injections), in combination with BUT (dose: 16 µmol/kg/day, via osmotic pumps) (*,$^{\#}$,$^{\delta}$p<0.05; **,$^{\#\#}$p<0.01; ***,$^{\#\#\#}$p<0.001; ****,$^{\#\#\#\#}$,$^{\delta\delta\delta\delta}$p<0.0001, n = 8-12. Statistics done using unpaired Student's *t*-test, with Holm-Sidak correction. *PBS versus PEGyAMPH; $^{\#}$PBS versus AMPH; $^{\delta}$PEGyAMPH versus AMPH.) Data presented as mean ± S.E.M. See also Figure S7.

Hence, treatment with PEGyAMPH protects mice against obesity by elevating thermogenesis coupled to heat dissipation, the latter of which relies on vasodilation/smooth muscle relaxation and is well known to be driven by ADRB2 (Chruscinski et al., 1999; Ernande et al., 2016). Consistently, we discovered that the anti-obesity effect of PEGyAMPH is completely abrogated by a selective ADRB2 antagonist (butoxamine, delivered via osmotic pumps - **Fig. 7. H-I**), further validating that this pathway is important for PEGyAMPH's metabolic effects.

Altogether, these results confirm that PEGyAMPH is a peripheral *sympathofacilitator* anti-obesity drug that activates a whole-body energy sink by coupling thermogenesis to heat dissipation without inducing behavioural changes nor cardiotoxicity.

## Discussion

The primary mechanism of action that underlies the anti-obesity effect of AMPH-based drugs, such as FDA-approved phentermine, is based on an effect in the brain that conveys pronounced behavioural effects: anorexia and hyperkinesia. Phentermine is a centrally acting anorexigenic drug that was developed as a less addictive option to other AMPH forms. However, studies in rodents have suggested that the anti-obesity effects of AMPHs and other anorexigenic drugs are partly, or even entirely, a result of non-behavioural factors (Arch, 1981; Herling et al., 2008). Although anorexia unquestionably reduces BW, our results indicate that this effect depends on an intact sympathetic axis (Pereira et al., 2017). As ADRB3 was described to be the main receptor mediating adrenergic-stimulated lipolysis in rodent adipocytes (Bloom et al., 1992; Guerra et al., 1998; Himms-Hagen et al., 1994; Susulic et al., 1995; Xiao et al., 2015), direct sympathomimetic agents, such as the ADRB3 agonist CL-316,243, were once regarded as potential anti-obesity therapies. However, as human lipolysis is mainly mediated by the other β-adrenoreceptors, ADRB3 agonists failed as anti-obesity therapies, and they are instead indicated for urogenital conditions (Arch, 2011; Lafontan and Berlan, 1993; Ursino et al., 2009). Direct thermogenic drugs such as compound 2,4-dinitrophenol, a mitochondrial uncoupler, were very effective anti-obesity treatments through converting energy to heat, but they also cause substantial side effects, including life-threatening hyperthermia (Harper et al., 2001). The historical failure of post-synaptic targeting in adipose tissue is suggestive of an orchestrated multi-pathway and multi-organ programme that is pre-synaptically controlled by the SNS (Bartness et al., 2014; Mahú and Domingos, 2017; Zeng et al., 2015). Thus, we reasoned that a pre-synaptic facilitation of sympathetic output would have a more potent effect, as SNS circuits would simultaneously activate multiple pathways, not only in WAT, but also in BAT and other metabolically relevant organs.

Indirect sympathomimetics, such as FDA-approved phentermine, demonstrated higher anti-obesity efficacy relative to the direct class but have prohibitive cardio-excitatory effects. However, whether this side effect is mediated via the brain or periphery has never been experimentally tested. We herein address this by testing the first-in-class exclusively peripheral AMPH, which does not enter the brain and is devoid of cardiovascular side effects. We reasoned that PEGylation of AMPH would render the molecule sufficiently big and impermeable to the brain. PEGylation is widely used as a stabilizer that alters the biodistribution of compounds in circulation

(Veronese, 2001), but whether it would successfully prevent brain access was uncertain, as variable BBB permeability has been reported in the literature depending on the molecule to be chemically modified (Pereira et al., 2017; Veronese, 2001). By using mass spectrometry of brain extracts, we document that PEGyAMPH does not reach the brain, yet it retains its ability to facilitate the activation of sympathetic neurons *in vitro* and *in vivo*, thus constituting the first in class of a peripheral *sympathofacilitator* with an anti-obesity action. PEGyAMPH reduces obesity with a size effect comparable to that of AMPH, yet with a distinct mechanism in that it spares effects relating to brain action, such as anorexia, hyperkinesia, and tremor. It also spares tachycardia and hypertension, and this could not be expected unless experimentally demonstrated, as we have done here. This distinction could be related to different molecular targets: unlike AMPH, PEGyAMPH does not bind Slc6a2, likely due to the loss of the amine group. Importantly, this group is not essential for interaction with the ADRB2, which we demonstrate to mediate the *sympathofacilitatory* and anti-obesity effect of PEGyAMPH. Elevation of SNS tone both to WAT and BAT activates lipolysis and thermogenesis (Bartness et al., 2014; Contreras et al., 2017; Hausberg et al., 2002; Mahú and Domingos, 2017; Zeng et al., 2015). Simultaneously, ADRB2 agonism is well known to lead to smooth muscle relaxation and vasodilation, which bode well to mediate the cardioprotective actions of PEGyAMPH, as well as its effect on thermal dissipation. Consistently, others have shown that the ADRB2-selective agonist salbutamol, increases BAT vasodilation and tissue perfusion, activating thermogenesis without directly targeting brown adipocytes (Ernande et al., 2016). The authors of this report did not assess changes in peripheral vasculature, and we did not probe BAT perfusion, but it is quite possible that PEGyAMPH might also increase blood flow to this tissue, further boosting thermogenesis. Moreover, although the relationship between peripheral vascular tone and cardiac function is undebatable (Delong and Sharma, 2019), the effect of blood flow on heat dissipation and its connection to metabolic regulation has only recently began to be appreciated as an important component of adiposity control. In fact, compensatory thermoregulation seems to drive hypermetabolic phenotypes in animals with genetic manipulations that facilitate heat dissipation (Kasza et al., 2019; Warner and Mittag, 2014; Warner et al., 2013).

Our results put forward the idea that coupling increased thermogenesis with peripheral heat dissipation, constitutes a sink for EE without causing hyperthermia and that AMPH-like compounds, such as FDA-approved phentermine or ADRB2 agonists, which are not indicated for long-term systemic use due to serious side effects, could be reformulated to become brain impermeable. Overall, our results are a proof-of-principle that peripheral *sympathofacilitators* could be a new generation of anti-obesity compounds that circumvent difficulties caused by BBB permeability and avoid brain-related side effects, including those relating to cardiovascular function.

**Acknowledgments:**

We thank the funding agencies listed below for supporting the laboratories in which the research was conducted. The authors thank Vikki Cantrill and Chelsea Larabee for her help with the preparation and editing of this manuscript.

**Funding:**

This work was supported by the Fundação para a Ciência e Tecnologia (FCT - PTDC-BIM-MET-3750-2014), the European Molecular Biology Organization (EMBO - Installation Grant 3037), the Human Frontier Science Program (HFSP - RGY0070/2016), Maratona da Saúde (Diabetes - 2016), and the Howard Hughes Medical Institute (HHMI - 208576/Z/17/Z). G.J.L.B. is a Royal Society University Research Fellow (UF110046 and URF\R\180019), FCT Investigator (IF/00624/2015) and the recipient of an European Research Council (ERC) Starting Grant (676832). B.J and A.K. were supported by the BBSRC (BB/M027252/1/bbsrc). We also acknowledge the Portuguese Mass Spectrometry Network (LISBOA-01-0145-FEDER-022125), the Project EU_FT-ICR_MS, funded by the European Union Horizon 2020 research and innovation programme under grant agreement nr. 731077.The contribution of Y.S., M.O. and F.C. were supported by Ministerio de Ciencia, Innovación y Universidades (grant AGL2017-88801-P and RTI2018-099592-B-C21). The contribution of M.L was supported by the Xunta de Galicia (2015-CP079 and 2016-PG068); the Ministerio de Economía y Competitividad (MINECO) co-funded by the FEDER Program of EU (RTI2018-101840-B-I00 and BFU2015-70454-REDT/Adipoplast), the Atresmedia Corporación and the “la Caixa” Banking Foundation under the project code HR18-00155. I.M. (PD/BD/52437/2013), A.B. (SFRH/BPD/96794/2013), P.M.S.D.C. (SFRH/BPD/103172/2014) and S.H.V. (SFRH/BPD/81627/2011) were supported by FCT; N.M.S. (ED481B 2016/168-0) was supported by Xunta de Galicia and E.R.P. (BES-2015-072743) was supported by Ministerio de Economía y Competitividad (MINECO).

**Author contributions:**

I.M. and A.I.D. conceived the experimental strategy; I.M. performed the sympathectomies and conducted the metabolic tests *in vivo*; I.M., R.M., M.O. and Y.S. performed the cardiovascular measurements and analysis; I.M., E.S., N.M.S., R.M. C.T., M.F.C., and V.G. treated the mice; tissue extractions and processing was performed by I.M., E.S., M.F.C., C.T., N.M.S., V.G. and R.M; I.M. performed the biochemical and gene expression measurements; M.F.C. and R.M. filmed and quantified the locomotor activity from video tracking; A.B. performed the *in vitro* cultures of sympathetic neurons; A.B. and S.H.V conducted the patch-clamp and calcium imaging recordings; A.M.S discussed neuronal excitability data; N.M.S., E.R.P. and M.L. performed and analysed the TSE measurements; Temperatures of BAT and Tail were probed and quantified by I.M., N.M.S., E.R.P. and M.L.; PEGylation of amphetamine was performed by P.M.S.D.C.; B.J. and A.K. performed the quantitative mass spectrometry based analysis of the drugs in plasma and tissues; FT-ICR mass spectrometry analysis was performed by P.M.S.D.C. and C.C.; F.C. performed the docking and molecular mechanics calculations; N.K. labelled and imaged the sympathetic neurons in culture; rodent husbandry was performed by R.M., C.T., V.G., N.K. and I.M.[&]; G.J.L.B. and M.M.A.P conceived the drug modification; I.M. and A.I.D. wrote the manuscript; all authors revised the manuscript and G.J.L.B. and A.I.D. are co-senior authors of this work.

**Competing interests:** A provisional patent to protect PEGyAMPH has been filed by Fundação Calouste Gulbenkian and Instituto de Medicina Molecular, which lists A.I.D. and G.J.L.B. as inventors. The remaining authors declare no competing interests.

**Data and materials availability:** All data that support the findings herein presented are available from the corresponding author upon reasonable request. We developed a PEGylated version of amphetamine, for which the reaction protocol is described in the methods section. The modified drug can be produced and purchased at WuXi AppTech upon request for research purposes only.

## Methods

**PEGylation of Amphetamine (PEGyAMPH synthesis)**. Inspired by Yang et al., 2009. Briefly, in a round-bottom flask *(R)*-1-phenylprop-2-ylamine hydrochloride salt (103 mg, 0.6 mmol, 2 equiv., Asiba Pharmatec.) was placed under inert atmosphere. A solution of methyl-PEG-NHS-ester reagent (1.1 mL, 100 mg, 0.39 mmol, 1 equiv., Thermo Scientific) in DMSO was then added, followed by the addition of diisopropylethylamine (DIPEA, 105 µL, 0.6 mmol, 2 eq, Sigma-Aldrich). The reaction was stirred at room temperature for 46 h, after which a multiple extraction with water/ethyl acetate was performed to remove the product from DMSO. Then preparative chromatography (5% EtOAc in MeOH, v/v) was performed to isolate compound PEGyAMPH in 98% yield (0.1 g). Characterization: **$^{1}$H NMR (300 MHz, $CDCl_3$)** δ 7.25 – 7.11 (m, 5H), 6.53 – 6.26 (m, 1H), 4.19 (p, *J* = 6.8 Hz, 1H), 3.63 – 3.47 (m, 14H), 3.32 (s, 3H), 2.79 (dd, *J* = 13.5, 6.1 Hz, 1H), 2.65 (dd, *J* = 13.5, 7.1 Hz, 1H), 2.37 (t, *J* = 6.4 Hz, 2H), 1.06 (d, *J* = 6.6 Hz, 3H) ppm. **$^{13}$C NMR (75 MHz, $CDCl_3$)** δ 170.92, 138.38, 129.55, 128.36, 126.40, 72.01, 70.70, 70.60, 70.46, 70.34, 67.43, 59.11, 46.02, 42.60, 37.21 ppm. **HRMS**: $[M+H]^{+}_{calc}$ = 354.22750; $[M+H]^{+}_{real}$ = 354.22783 (error –0.9 ppm). Scale-up of the reaction for chronic *in vivo* treatments was reproduced by Wuxi AppTec.

**Mice and housing conditions.** Mice were housed at controlled temperature and humidity, under a 12 h light/dark cycle. Food and water were supplied *ad libitum*, unless mentioned otherwise. The animal experiments were performed in agreement with the International Law on Animal Experimentation and were approved by the IGC ethics committee and by the USC Ethical Committee (Project ID 15010/14/006). C57BL/6 mice were obtained from the Mice Production Facility at the IGC. *TH-cre* (Jax, #008601), CAG-LSL-*GCaMP3* (Jax, #014538), LSL-*DTR* (Jax, #007900), mice were purchased from Jackson Laboratory, and bred to produce homozygous *TH-cre;* CAG-LSL-*GCaMP3* and *TH-cre;* LSL-*DTR* mice. LSL-*DTR* mice were used as controls for the sympathectomization studies.

**PEGyDT-mediated regional sympathectomy.** For detailed characterization refer to Pereira *et al.* 2017. Briefly, 7-8 weeks old *TH-cre;* LSL-*DTR* male mice were used for genetic-sympathectomy experiments and aged-matched LSL-*DTR* were used as controls. PEGylated Diphtheria Toxin (PEGyDT) was administered once a day for 8 consecutive days (25 ng/g of BW, IP injections, diluted in PBS). All following experiments were performed at least 24 h after the last injection.

**High-fat diet challenge and chronic treatments.** All mice used for DIO challenges and follow-up metabolic analysis were males. When C57BL/6 mice reached 8 weeks of age, or 1 day after sympathectomy protocol was performed in both *TH-cre; LSL-DTR* and respective controls *LSL-DTR*, normal diet was replaced with high fat diet (HFD, Ssniff, Spezialdiäten, Soest, Germany, D12492) concomitantly with treatment of either AMPH or PEGyAMPH (dose: 120 µmol/kg of BW for both drugs diluted in PBS, daily IP injections). Length of exposure to HFD and treatment is indicated in figure legends.

**Intracerebroventricular treatments.** Intracerebroventricular (ICV) cannulae were stereotaxically implanted under a mix of inhaled isoflurane and oxygen, using the following coordinates 1.5 mm lateral to bregma, 0.6 mm posterior, 4.0 mm deep. Mice equipped with ICV cannulae were given 7 days to recover before injections and measurements. A bolus ICV injection of AMPH or PEGyAMPH (60 nmol, diluted in 5 µL of PBS), or of PBS as control was acutely administrated for behavioural and cardiorespiratory measurements as described below.

**Non-invasive Cardiovascular Measurements.** Blood Pressure and Heart Rate were measured from awake restrained animals using a Volume Pressure Recording (VPR) sensor and tail-cuff system (CODA, Kent Scientific Corporation). To prevent stress-related effects, mice were trained for a minimum of 3 days before measurements. At least 15 accurate measurements per animal were used for analysis of diastolic, mean and systolic pressure and at least 8 for analysis of the heart rate. Baseline was recorded just before injection, and the effect of the drugs was measured 15-30 min post injection with PBS, AMPH or PEGyAMPH (dose: 120 µmol/kg of BW for both drugs, daily IP injections).

**Infrared pulse oximetry.** The day before measurements the hair around the neck of each mouse was removed using Veet cream (Unilever). 24-48h post-depilation, the cardiopulmonary status of each mouse was analyzed by MouseOx Plus (Starr Life Sciences Corp) in accordance with manufacturer's instructions. Each mouse was very briefly anaesthetised using 5% isoflurane to facilitate placement of a CollarClip Sensor, and allowed to acclimatize to the anesthesia with 1-2% isoflurane for 5 min. This time window was sufficient for animals to recover normal activities and physiological readings. Measurements were then recorded for 5-10 min at baseline and then for another 10-15min after injections (IP of PEGyAMPH and AMPH, dose: 120 µmol/kg of BW for both drugs; or ICV of PBS and AMPH, dose: 60nmol, bolus per animal). The time points described were used to collect representative, error-free data due to the motion artefact (DeMeulenaere, 2007).

**Locomotion assays.** After 3 weeks of HFD exposure and treatment, mice were acclimated to tracking cages for 1 week before starting the 72h locomotion measurements by using a high throughput tracking system (LabMaster, TSE Systems). Animals were also filmed for 20-30 min, with a ZEISS optics camera 1 h post injection inside their normal housing cage, for assessment of total distance travelled. Footage-records were filtered by using video editor Avidemux (Avidemux 2.7.1) and 10-15 min distance computations were quantified with the TrackMate tracking plugin from Fiji (Fiji; Wisconsin-Madinson).

**Calorimetry assays.** Animals were analysed for Energy Expenditure (EE) using a calorimetric system (LabMaster; TSE Systems). Animals were placed in a temperature-controlled (24°C) box through which air was pumped. After calibrating the system with the reference gases (20.9% $O_2$,

0.05% $CO_2$ and 79.05% $N_2$), the metabolic rate was measured for 2-3 days, and EE was recorded every 30 min. Animals were placed for adaptation for 1 week before starting the measurements. Normalized EE was calculated as described in Tschöp et al. (2012) and the distribution curves were obtained using the CalR Web-based tool (Mina et al., 2018).

**Glucose metabolism tests.** For the intraperitoneal Glucose Tolerance Test (GTT), mice were injected with PBS, AMPH or PEGyAMPH and then fasted for 6 h, before being given 2 g glucose/kg of BW, IP. Blood was drawn from the tail vein and glucose levels were measured using a glucometer (Accu-Check System, Roche) at 0, 15, 30, 60, 90, and 120 min after glucose administration. For the Insulin Tolerance Test (ITT), mice were injected with PBS, AMPH or PEGyAMPH and then fasted for 2 h, before being given (IP) 0.9U/kg of BW, IP, of recombinant human insulin (Sigma), blood glucose levels were measured at 0, 15, 30, 60, 90, 120, 150 and 180 min after insulin administration.

**Thermoregulation studies.** All measurements were done in *ad libitum* fed mice 2 h post-injections with PBS, AMPH or PEGyAMPH. Rectal temperature was measured with an electronic thermometer (Precision). BAT and Tail thermographic pictures were taken with a Compact-Infrared-Thermal-Imaging-Camera (FLIR; West Malling) and FLIR-Tools-Software (FLIR; West Malling), to quantify local temperature (Martínez-Sánchez et al., 2017).

**Blood and Plasma analysis**. Blood was collected from the tail vein of HFD fed mice, 2 h post-injections with PBS, AMPH or PEGyAMPH, without access to food. Blood glucose was measured with a glucometer (Accu-Check, Roche). Analysis of Insulin, Triglycerides, Glycerol and FFA levels in plasma was performed by using Mouse Ultrasensitive Insulin ELISA (Alpco), Triglyceride Quantification Kit (Abcam), Free Glycerol Reagent (Sigma) and Glycerol Standard Solution (Sigma), and Free Fatty Acid Quantification Kit (MAK044, Sigma), respectively according to manufacturer's instructions**.**

**Tissue NE measurements (ELISA).** To assess peripheral NE content in tissues, mice were sacrificed in *ad libitum* conditions 2 h post injection with PBS, AMPH or PEGyAMPH. NE levels were determined with a NE ELISA kit (Labor Diagnostika Nord GmbH). Tissues were homogenized and sonicated in homogenization buffer (1 M HCl, 1 mM EDTA, 4 mM sodium metabisulfite), and cellular debris was pelleted by centrifugation at 20,000 g for 10 min at 4 ºC). All tissue samples were normalized to total tissue protein concentration, measured with Quick Start Bradford protein assay (Bio-Rad), according to manufacturer's instructions.

**Fecal output assay.** 24 h fecal output was collected and weighed. The feces were washed with 1x PBS and total triglyceride content was extracted by homogenization and boiling, for 2 cycles of 5 min, in 5% NP-40. Triglyceride content was measured using Triglyceride Quantification Kit (Abcam), according to manufacturer's instructions, and normalized to the weight of total fecal output.

**Tissue Triglycerides Analysis.** To assess gastrocnemius muscle and liver content in tissues, mice were sacrificed in *ad libitum* conditions 2 h post injection with PBS, AMPH or PEGyAMPH. Triglyceride content was measured using Triglyceride Quantification Kit (Abcam), according to manufacturer's instructions. Tissue samples were normalized to total tissue protein concentration, measured with Quick Start Bradford protein assay (Bio-Rad), according to manufacturer's instructions.

**Quantitative PCR.** For gene expression analysis mice were sacrificed in *ad libitum* conditions 2 h post injection with PBS, AMPH or PEGyAMPH, tissues were collected and immediately frozen. Total tissue RNA was extracted by using PureLink RNA Mini Hit (Invitrogen) according to manufacturer's instructions, from which complementary DNA was reverse-transcribed by using SuperScript II (Invitrogen) and random primers (Invitrogen). Quantitative PCR was performed with SYBR Green (Applied Biosystems) in ABI QuantStudio 7 (Applied Biosystems). Glyceraldehyde 3-phosphate dehydrogenase (*GAPDH*) was used as housekeeping gene to normalize liver and gastrocnemius muscle tissue samples. Acidic ribosomal phosphoprotein P0 (*Arbp0*) was used as housekeeping gene to normalize adipose tissues samples. The list of primers used is shown in Supplementary Table 1.

**SCG neurons culture and treatments.** Primary cultures of SCG neurons were performed from postnatal day 30 C57BL/6 or *TH-cre;* CAG-LSL-*GCaMP3* mice (male and female). After decapitation, both SCG of each animal were removed and cleaned of all visible adipose tissue and surrounding connective tissue before transfer to Dulbecco's Modified Eagle Medium (Biowest). Then, SCG were treated enzymatically in two steps to yield single neurons in accordance to the method described by Motagally and collaborators (Motagally et al., 2009), with some modifications. First, SCG were subjected to enzymatic dissociation in 2.5 mg/mL collagenase solution (Sigma-Aldrich) in Hank's Balanced Salt Solution (HBSS) without calcium and magnesium (Gibco, Life Technologies) at 37 ºC with agitation, followed by 0.25% trypsin solution (Biowest) in PBS at 37 ºC with agitation. SCG was then mechanically dissociated into a suspension of single cells. The isolated sympathetic neurons were plated, 2500 cells per coverslip (6 mm) coated with poly-d-lysine (Sigma) and growth factor-reduced Matrigel (BD Biosciences) and cultured in Neurobasal medium (Gibco) supplemented with 2% B-27 (Gibco), 10% fetal bovine serum (Gibco), 1% penicillin/streptomycin (Biowest), 100 ng/mL nerve growth factor (AbD Serotec) and 5 µM 5-fluoro-2'-deoxyuridine (Sigma-Aldrich). Cells were kept in culture for 6 days *in vitro* (DIV) at 37 ºC with 5% $CO_2$ conditioned atmosphere to obtain an enriched culture of sympathetic neurons. Before measurements, neurons were incubated with 15 µM AMPH or 15 µM PEGyAMPH for 24 h at 37 ºC with 5% $CO_2$ conditioned atmosphere. Butoxamine (Santa-Cruz Biotechnology) was add at a concentration of 10µM, 30min prior to the calcium-imaging experiments.

**Intracellular Calcium-Imaging.** For $Ca^{2+}$ experiments, sympathetic neurons were obtained from *TH-cre;* CAG-LSL-*GCaMP3* mice. At 7 DIV, coverslips with sympathetic neurons from GCaMP3$^{+}$ mice were mounted on an inverted microscope with epifluorescent optics (Axiovert 135TV, Zeiss) equipped with a xenon lamp (located at a Lambda DG-4, Sutter Instrument) and band-pass filter of 450-490 nm wavelengths. $Ca^{2+}$ measurements were performed at 37 ºC, as reported in (Jacob et al., 2014). Throughout the experiments the Ach was applied focally through a drug-filled micropipette placed under visual guidance over a single neuronal cell. Drug release was performed by focal pressure (10 psi for 40 s) through a Toohey Spritzer pressure System IIe (Toohey Company). Pressure application of external physiological solution did not cause any measurable change in intracellular $Ca^{2+}$ concentration. Images were obtained every 250 ms by exciting the preparations at 450-490 nm and the emission wavelength was set to 510 nm. Neurons were imaged with a cooled CCD camera (Photometrics CoolSNAP fx), processed and analysed

by using the software MetaFluor (Universal Imaging, West Chester, PA). $Ca^{2+}$ levels were recorded at the cell body of neurons (manually defined over the cell profile) in the field of view and variations were estimated as changes of the fluorescence signal over the baseline ($\Delta F/F0 = [(F_{post} - F_{rest})/F_{rest}]$).

**Electrophysiology.** Whole cell patch-clamp recordings performed at 7 DIV in dissociated cultures of sympathetic neurons from C57BL/6 mice using an upright microscope (Zeiss Axioskop 2FS) equipped with differential interference contrast optics by using a Zeiss AxioCam MRm camera and a x40 IR-Achroplan objective. During recordings, cells were continuously superfused with artificial cerebrospinal fluid containing (in mM: 124 NaCl, 3 KCl, 1.2 $NaH_2PO_4$, 25 $NaHCO_3$, 2 $CaCl_2$, 1 $MgSO_4$ and 10 glucose), which was continuously gassed with 95% $O_2$/5% $CO_2$. Recordings were performed at room temperature in current-clamp or voltage-clamp mode [holding potential (Vh) = -60 mV] with an Axopatch 200B amplifier (Axon Instruments)(Félix-Oliveira et al., 2014). Briefly, patch pipettes with 4 to 7 MΩ resistance when filled with an internal solution (containing (in mM): 125 K-gluconate, 11 KCl, 0.1 $CaCl_2$, 2 $MgCl_2$, 1 EGTA, 10 HEPES, 2 MgATP, 0.3 NaGTP, and 10 phosphocreatine, pH 7.3, adjusted with 1 M NaOH, 280-290 mOsm) were used to record excitatory synaptic currents and action potential activity. The junction potential was not compensated for, and offset potentials were nulled before gigaseal formation. The resting membrane potential was measured immediately upon establishing whole cell configuration. Firing patterns of sympathetic neurons were then immediately assessed in current-clamp mode by injection of 500 ms current pulses (-25–275 pA in 12.5 or 25 pA increments) from an initial holding potential (Vh) of −70 mV. For each neuron, the threshold for action potential generation was determined by membrane potential at which phase plot slope reached 10 mV/ms (Naundorf et al., 2005). For each neuron, Δ depolarization for AP firing was calculated as the difference between the resting membrane potential and the threshold for action potential generation.

**Fourier-transform ion cyclotron resonance (FT-ICR) mass spectrometry.** 12 weeks old male C57BL/6 mice were injected IP and sacrificed 30 min post-injection with AMPH or PEGyAMPH (dose: 120 µmol/kg of BW for both drugs). Brain samples were snap-frozen in liquid nitrogen before extraction procedures (Agudelo et al., 2014). Whole brain samples were smashed and extracted using ice-cold 1 mM perchloric acid (500 µL per sample) and left extracting overnight. After this time, the samples were centrifuged twice for 20 min at 5000 rpm, 4 ºC. Supernatants were transferred to new vials, frozen and freeze dried overnight each time, concentrated to 50 µL. Then, 25 µL of the remaining solutions were diluted in 75 µL of an electrospray ionization solution ($CH_3CN$:$H_2O$, 3:1). The samples were then evaluated through direct injection by using a Fourier-transform ion cyclotron resonance (FT-ICR) mass spectrometer (Bruker Apex Ultra, 7 Tesla actively shielded magnet).

**Quantitative liquid chromatography with mass spectrometry detection.** 8-12 weeks old C57BL/6 mice were injected IP and sacrificed 30 min post-injection with AMPH or PEGyAMPH (dose: 120 µmol/kg of BW for both drugs). Plasma and tissue samples were snap-frozen in liquid nitrogen upon collection and extraction procedures were prepared by a protein crash method for the extraction and quantitative analysis of drug content. Briefly, around 100 mg of tissue (brain and heart) were added to 100 µL of water inside a plastic screw-cap Eppendorf vial, followed by the addition of 100 µL of the stable isotope amphetamine internal standard (Amphetamine-d11 at

100 nM in water). Then a 5 mm stainless steel ball bearing was added to each sample. The samples were then homogenized using a Bioprep-24-1004 homogenizer (Allsheng, Hangzhou City, China) run at speed; 5 m/s, time; 30 seconds for 2 cycles. Then, 250 µL of acetone was added to each sample to precipitate any proteins in the solution. The samples were thoroughly vortexed to ensure optimal analyte recovery (recovery was >75 %). The samples were then centrifuged (5 min at ~20,000 g) to produce a clear supernatant separate from any solid particles. The supernatant was then transferred in to a separate 2 mL amber glass auto-sampler vial (Agilent Technologies, Santa Clara California, USA). The acetone solvent was then evaporated-off by concentrating the sample on an Eppendorf Concentrator Plus system (Eppendorf, Stevenage, UK) run for 20 minutes at 60 degree Celsius. The remaining sample (~200 µL) was then transferred into a 300 µL low-volume vial insert inside a 2 mL amber glass auto-sample vial ready for liquid chromatography with mass spectrometry detection (LC-MS). Full chromatographic separation of the analytes (AMPH and PEGyAMPH) was achieved using Shimadzu HPLC System (Shimadzu UK Limited, Milton Keynes, United Kingdom) with the injection of 5 µL onto a Waters Acquity UPLC® BEH C18 column; 1.7 µm, I.D. 2.1 mm X 50 mm, maintained at 40 °C. Mobile phase A was water with 0.1% formic acid. Mobile phase B was acetonitrile with 0.1% formic acid. The flow was maintained at 500 µL per minute through the following gradient: 0.00 minutes_1% mobile phase B; 1.00 min, 1% mobile phase B; 2.00 min, 95% mobile phase B; 3.30 min, 95% mobile phase B; 3.40 min, 1% mobile phase B; 6.50 min, 1% mobile phase B. The sample injection needle was washed using acetonitrile with 0.1 % formic acid. The mass spectrometer (MS) used was the Thermo Scientific Exactive Orbitrap with a heated electrospray ionization source (Thermo Fisher Scientific, Hemel Hempstead, UK). The mass spectrometer was calibrated immediately before sample analysis using positive and negative ionization calibration solution (recommended by Thermo Scientific). Additionally, the heated electrospray ionization source tune files were optimized for both AMPH and PEGyAMPH independently and applied to the mass spectrometry method by segmenting the MS method; this produced the lowest limit of quantitation for each compound. AMPH segment 1 was run in positive mode from 0 to 2.9 minutes with the mass spectrometer resolution set to 50,000 with a full-scan range of m/z 60 to 1200 Da. PEGyAMPH segment 2 was run in positive mode from 2.9 to 5 minutes with the mass spectrometer resolution set to 50,000 with a full-scan range of m/z 60 to 1200 Da. Analyte quantification was achieved by extracting the expected analyte masses (AMPH: 136.11208 [M+H]+ and 119.0861 [M+H-NH3]+ at retention time 2.73 minutes; AMPH-d11: 147.18112 [M+H]+ and 130.1551 [M+H-NH3]+ at retention time 2.72 minutes; PEGyAMPH: 354.22750 [M+H]+ at retention time 3.12 minutes). The area under the curve of these high resolution extracted ion chromatograms (with a window of ± 8 ppm) were normalized to the internal standard (amphetamine-d11) to account for extraction and instrument variations and then compared to a quantitative calibration line (lower limit of quantitation: 10 nM; upper limit of quantitation: 1,000 nM, for both compounds). The calculated concentrations of the analytes were then divided by the amount of tissue used in the extraction protocol to give the final results in nM per mg of tissue extracted (nM/mg).

**Docking calculations and Molecular Mechanics minimizations.** The X-ray structure reported of $\beta_2$-adrenoceptor in complex to adrenaline (pdb ID: 4LDO) (Ring et al., 2013) was used as a 3D model. The Docking calculations between the ligands and the receptor were performed with

PatchDock Server and FireDock (Schneidman-Duhovny et al., 2005). Molecular mechanics minimizations were then carried out on the complexes using AMBER 18 package, (D. A. Case, I. Y. Ben-Shalom, S. R. Brozell, D. S. Cerutti, T. E. Cheatham, III, V. W. D. Cruzeiro, T. A. Darden, R. E. Duke, D. Ghoreishi, M. K. Gilson, H. Gohlke, A. W. Goetz, D. Greene, R Harris, N. Homeyer, Y. Huang,S. Izadi, A. Kovalenko, T. Kurtzman, T. S. Lee, S. LeGrand, P. Li, C. Lin, J. Liu, T. Luchko, R. Luo, D. J.Mermelstein, K. M. Merz, Y. Miao, G. Monard, C. Nguyen, H. Nguyen, I. Omelyan, A. Onufriev, F. Pan, R. Qi, D. R. Roe, A. Roitberg, C. Sagui, S. Schott-Verdugo, J. Shen, C. L. Simmerling, J. Smith, R. Salomon Ferrer, J. Swails, R. C. Walker, J. Wang, H. Wei, R. M. Wolf, X. Wu, L. Xiao, D. M. York and P.A. Kollman (2018), AMBER 2018, *University of California, San Francisco*), which was implemented with ff14SB (Maier et al., 2015) and GAFF (Wang et al., 2004) force fields. Parameters for the ligands (AMPH and PEGyAMPH) were generated with the antechamber module of AMBER, using GAFF force field and with partial charges set to fit the electrostatic potential generated with HF/6-31G(d) by RESP (Bayly et al., 1993). The charges were calculated according to the Merz-Singh-Kollman scheme using Gaussian 16.( Frisch, M. J.; Trucks, G. W.; Schlegel, H. B.; Scuseria, G. E.; Robb, M. A.; Cheeseman, J. R.; Scalmani, G.; Barone, V.; Petersson, G. A.; Nakatsuji, H.; et al. *Gaussian 16 rev. B.01,* 2016, Wallingford, CT) The complexes were immersed in a water box with a 10 Å buffer of TIP3P water molecules (Jorgensen et al., 1983) and neutralized by adding explicit counter ions. A two-stage geometry optimization approach was performed with a total of 5000 minimization steps and using the default settings of AMBER 18. The first stage minimizes only the positions of solvent molecules and ions, and the second stage is an unrestrained minimization of all the atoms in the system.

**Histopathological analyses.** Mouse tissues were fixed in buffered formalin, and inclusion in paraffin was done according to standard technical procedures. Histopathology studies were performed on formalin-fixed and paraffin-embedded sections of 3–6 µm thick for Haematoxylin and Eosin. Tissues were analysed with a Leica DM LB2 microscope, and images captured with a Leica DFC 250 camera.

**Statistics.** The number of animals used in each experimental setting and the analysis performed are specified in each figure legend. Statistical analyses were performed with GraphPad Prism software (San Diego, CA) using unpaired Student's *t*-test (two-tailed) when two groups were being compared or one-way ANOVA when several groups were being compared. One-way ANOVA was followed by was followed by Bonferroni multiple-comparisons test with one group indicated as a control group. $p < 0.05$ was considered statistically significant. Data are represented as mean ± S.E.M. Data displayed normal variance.

**References:**


Agudelo, L.Z., Femenía, T., Orhan, F., Porsmyr-Palmertz, M., Goiny, M., Martinez-Redondo, V., Correia, J.C., Izadi, M., Bhat, M., Schuppe-Koistinen, I., et al. (2014). Skeletal Muscle PGC-1α1 Modulates Kynurenine Metabolism and Mediates Resilience to Stress-Induced Depression. Cell *159*, 33–45.

Arch, J.R.S. (1981). The contribution of increased thermogenesis to the effect of anorectic drugs on body composition in mice. Am. J. Clin. Nutr. *34*, 2763–2769.

Arch, J.R.S. (2011). Challenges in $\beta_3$-adrenoceptor agonist drug development. Ther. Adv. Endocrinol. Metab. *2*, 59–64.

Arch, J.R.S., and Trayhurn, P. (2013). Detection of thermogenesis in rodents in response to anti-obesity drugs and genetic modification. Front. Physiol. *4*.

Bartness, T.J., Liu, Y., Shrestha, Y.B., and Ryu, V. (2014). Neural innervation of white adipose tissue and the control of lipolysis. Front. Neuroendocrinol. *35*, 473–493.

Bayly, C.I., Cieplak, P., Cornell, W., and Kollman, P.A. (1993). A well-behaved electrostatic potential based method using charge restraints for deriving atomic charges: the RESP model. J. Phys. Chem. *97*, 10269–10280.

Blessing, W., McAllen, R., and McKinley, M. (2016). Control of the Cutaneous Circulation by the Central Nervous System. Compr. Physiol. *6*, 1161–1197.

Bloom, J.D., Dutia, M.D., Johnson, B.D., Wissner, A., Burns, M.G., Largis, E.E., Dolan, J.A., and Claus, T.H. (1992). Disodium (R,R)-5-[2-[[2-(3-chlorophenyl)-2-hydroxyethyl]-amino] propyl]-1,3-benzodioxole-2,2-dicarboxylate (CL 316,243). A potent beta-adrenergic agonist virtually specific for beta 3 receptors. A promising antidiabetic and antiobesity agent. J. Med. Chem. *35*, 3081–3084.

Borbély, A.A., Baumann, I.R., and Waser, P.G. (1974). Amphetamine and thermoregulation: studies in the unrestrained and curarized rat. Naunyn. Schmiedebergs Arch. Pharmacol. *281*, 327–340.

Bray, G.A. (1991). Obesity, a disorder of nutrient partitioning: the MONA LISA hypothesis. J. Nutr. *121*, 1146–1162.

Burgess, S.C., He, T., Yan, Z., Lindner, J., Sherry, A.D., Malloy, C.R., Browning, J.D., and Magnuson, M.A. (2007). Cytosolic phosphoenolpyruvate carboxykinase does not solely control the rate of hepatic gluconeogenesis in the intact mouse liver. Cell Metab. *5*, 313–320.

Camell, C.D., Sander, J., Spadaro, O., Lee, A., Nguyen, K.Y., Wing, A., Goldberg, E.L., Youm, Y.-H., Brown, C.W., Elsworth, J., et al. (2017). Inflammasome-driven catecholamine catabolism in macrophages blunts lipolysis during ageing. Nature *550*, 119–123.

Caron, A., Lee, S., Elmquist, J.K., and Gautron, L. (2018). Leptin and brain–adipose crosstalks. Nat. Rev. Neurosci. *19*, 153–165.

Chruscinski, A.J., Rohrer, D.K., Schauble, E., Desai, K.H., Bernstein, D., and Kobilka, B.K. (1999). Targeted disruption of the beta2 adrenergic receptor gene. J. Biol. Chem. *274*, 16694–16700.

949 Contreras, C., Nogueiras, R., Diéguez, C., Rahmouni, K., and López, M. (2017). Traveling from
950 the hypothalamus to the adipose tissue: The thermogenic pathway. Redox Biol. *12*, 854–863.

951 Cooke, D., and Bloom, S. (2006). The obesity pipeline: current strategies in the development of
952 anti-obesity drugs. Nat. Rev. Drug Discov. *5*, 919–931.

953 Delong, C., and Sharma, S. (2019). Physiology, Peripheral Vascular Resistance. In StatPearls,
954 (Treasure Island (FL): StatPearls Publishing), p.

955 DeMeulenaere, S. (2007). Pulse Oximetry: Uses and Limitations. J. Nurse Pract. *3*, 312–317.

956 Ernande, L., Stanford, K.I., Thoonen, R., Zhang, H., Clerte, M., Hirshman, M.F., Goodyear, L.J.,
957 Bloch, K.D., Buys, E.S., and Scherrer-Crosbie, M. (2016). Relationship of brown adipose tissue
958 perfusion and function: a study through β2-adrenoreceptor stimulation. J. Appl. Physiol. *120*, 825–
959 832.

960 Félix-Oliveira, A., Dias, R.B., Colino-Oliveira, M., Rombo, D.M., and Sebastião, A.M. (2014).
961 Homeostatic plasticity induced by brief activity deprivation enhances long-term potentiation in the
962 mature rat hippocampus. J. Neurophysiol. *112*, 3012–3022.

963 Fischer, A.W., Hoefig, C.S., Abreu-Vieira, G., de Jong, J.M.A., Petrovic, N., Mittag, J., Cannon,
964 B., and Nedergaard, J. (2016). Leptin Raises Defended Body Temperature without Activating
965 Thermogenesis. Cell Rep. *14*, 1621–1631.

966 Gabanyi, I., Muller, P.A., Feighery, L., Oliveira, T.Y., Costa-Pinto, F.A., and Mucida, D. (2016).
967 Neuro-immune Interactions Drive Tissue Programming in Intestinal Macrophages. Cell *164*, 378–
968 391.

969 Geerling, J.J., Boon, M.R., Kooijman, S., Parlevliet, E.T., Havekes, L.M., Romijn, J.A., Meurs,
970 I.M., and Rensen, P.C.N. (2014). Sympathetic nervous system control of triglyceride metabolism:
971 novel concepts derived from recent studies. J. Lipid Res. *55*, 180–189.

972 Granneman, J.G., Burnazi, M., Zhu, Z., and Schwamb, L.A. (2003). White adipose tissue
973 contributes to UCP1-independent thermogenesis. Am. J. Physiol.-Endocrinol. Metab. *285*,
974 E1230–E1236.

975 Guerra, C., Koza, R.A., Yamashita, H., Walsh, K., and Kozak, L.P. (1998). Emergence of brown
976 adipocytes in white fat in mice is under genetic control. Effects on body weight and adiposity. J.
977 Clin. Invest. *102*, 412–420.

978 Harper, J.A., Dickinson, K., and Brand, M.D. (2001). Mitochondrial uncoupling as a target for drug
979 development for the treatment of obesity. Obes. Rev. Off. J. Int. Assoc. Study Obes. *2*, 255–265.

980 Harris, J.M., and Chess, R.B. (2003). Effect of pegylation on pharmaceuticals. Nat. Rev. Drug
981 Discov. *2*, 214–221.

982 Hausberg, M., Morgan, D.A., Mitchell, J.L., Sivitz, W.I., Mark, A.L., and Haynes, W.G. (2002).
983 Leptin potentiates thermogenic sympathetic responses to hypothermia: a receptor-mediated
984 effect. Diabetes *51*, 2434–2440.

985 Heal, D.J., Smith, S.L., Gosden, J., and Nutt, D.J. (2013). Amphetamine, past and present – a
986 pharmacological and clinical perspective. J. Psychopharmacol. (Oxf.) *27*, 479–496.

Herling, A.W., Kilp, S., Elvert, R., Haschke, G., and Kramer, W. (2008). Increased energy expenditure contributes more to the body weight-reducing effect of rimonabant than reduced food intake in candy-fed wistar rats. Endocrinology *149*, 2557–2566.

Himms-Hagen, J., Cui, J., Danforth, E., Taatjes, D.J., Lang, S.S., Waters, B.L., and Claus, T.H. (1994). Effect of CL-316,243, a thermogenic beta 3-agonist, on energy balance and brown and white adipose tissues in rats. Am. J. Physiol.-Regul. Integr. Comp. Physiol. *266*, R1371–R1382.

Ikeda, K., Kang, Q., Yoneshiro, T., Camporez, J.P., Maki, H., Homma, M., Shinoda, K., Chen, Y., Lu, X., Maretich, P., et al. (2017). UCP1-independent signaling involving SERCA2b-mediated calcium cycling regulates beige fat thermogenesis and systemic glucose homeostasis. Nat. Med. *23*, 1454–1465.

Ikeda, K., Maretich, P., and Kajimura, S. (2018). The Common and Distinct Features of Brown and Beige Adipocytes. Trends Endocrinol. Metab. *29*, 191–200.

Jacob, P.F., Vaz, S.H., Ribeiro, J.A., and Sebastião, A.M. (2014). P2Y $_1$ receptor inhibits GABA transport through a calcium signalling-dependent mechanism in rat cortical astrocytes: GATs Modulation by P2Y $_1$ Receptor in Rat Astrocytes. Glia *62*, 1211–1226.

Jéquier, E., Gygax, P.H., Pittet, P., and Vannotti, A. (1974). Increased thermal body insulation: relationship to the development of obesity. J. Appl. Physiol. *36*, 674–678.

Jorgensen, W.L., Chandrasekhar, J., Madura, J.D., Impey, R.W., and Klein, M.L. (1983). Comparison of simple potential functions for simulating liquid water. J. Chem. Phys. *79*, 926–935.

Jung, R.T., Shetty, P.S., James, W.P., Barrand, M.A., and Callingham, B.A. (1979). Reduced thermogenesis in obesity. Nature *279*, 322–323.

Kasza, I., Adler, D., Nelson, D.W., Eric Yen, C.-L., Dumas, S., Ntambi, J.M., MacDougald, O.A., Hernando, D., Porter, W.P., Best, F.A., et al. (2019). Evaporative cooling provides a major metabolic energy sink. Mol. Metab. *27*, 47–61.

Lafontan, M., and Berlan, M. (1993). Fat cell adrenergic receptors and the control of white and brown fat cell function. J. Lipid Res. *34*, 1057–1091.

Lee, P., Bova, R., Schofield, L., Bryant, W., Dieckmann, W., Slattery, A., Govendir, M.A., Emmett, L., and Greenfield, J.R. (2016). Brown Adipose Tissue Exhibits a Glucose-Responsive Thermogenic Biorhythm in Humans. Cell Metab. *23*, 602–609.

Mahú, I., and Domingos, A.I. (2017). The sympathetic neuro-adipose connection and the control of body weight. Exp. Cell Res. *360*, 27–30.

Maier, J.A., Martinez, C., Kasavajhala, K., Wickstrom, L., Hauser, K.E., and Simmerling, C. (2015). ff14SB: Improving the Accuracy of Protein Side Chain and Backbone Parameters from ff99SB. J. Chem. Theory Comput. *11*, 3696–3713.

Malpas, S.C. (2010). Sympathetic nervous system overactivity and its role in the development of cardiovascular disease. Physiol. Rev. *90*, 513–557.

Martínez-Sánchez, N., Seoane-Collazo, P., Contreras, C., Varela, L., Villarroya, J., Rial-Pensado, E., Buqué, X., Aurrekoetxea, I., Delgado, T.C., Vázquez-Martínez, R., et al. (2017). Hypothalamic

AMPK-ER Stress-JNK1 Axis Mediates the Central Actions of Thyroid Hormones on Energy Balance. Cell Metab. *26*, 212-229.e12.

Melnikova, I., and Wages, D. (2006). Anti-obesity therapies. Nat. Rev. Drug Discov. *5*, 369–370.

Mina, A.I., LeClair, R.A., LeClair, K.B., Cohen, D.E., Lantier, L., and Banks, A.S. (2018). CalR: A Web-Based Analysis Tool for Indirect Calorimetry Experiments. Cell Metab. *28*, 656-666.e1.

Morton, G.J., Muta, K., Kaiyala, K.J., Rojas, J.M., Scarlett, J.M., Matsen, M.E., Nelson, J.T., Acharya, N.K., Piccinini, F., Stefanovski, D., et al. (2017). Evidence That the Sympathetic Nervous System Elicits Rapid, Coordinated, and Reciprocal Adjustments of Insulin Secretion and Insulin Sensitivity During Cold Exposure. Diabetes *66*, 823–834.

Motagally, M.A., Lukewich, M.K., Chisholm, S.P., Neshat, S., and Lomax, A.E. (2009). Tumour necrosis factor α activates nuclear factor κB signalling to reduce N-type voltage-gated $Ca^{2+}$ current in postganglionic sympathetic neurons: $Ca^{2+}$ current inhibition by TNFα. J. Physiol. *587*, 2623–2634.

Naundorf, B., Geisel, T., and Wolf, F. (2005). Action Potential Onset Dynamics and the Response Speed of Neuronal Populations. J. Comput. Neurosci. *18*, 297–309.

Nonogaki, K. (2000). New insights into sympathetic regulation of glucose and fat metabolism. Diabetologia *43*, 533–549.

Pereira, M.M.A., Mahú, I., Seixas, E., Martinéz-Sánchez, N., Kubasova, N., Pirzgalska, R.M., Cohen, P., Dietrich, M.O., López, M., Bernardes, G.J.L., et al. (2017). A brain-sparing diphtheria toxin for chemical genetic ablation of peripheral cell lineages. Nat. Commun. *8*, 14967.

Petersen, M.C., Vatner, D.F., and Shulman, G.I. (2017). Regulation of hepatic glucose metabolism in health and disease. Nat. Rev. Endocrinol. *13*, 572–587.

Pirzgalska, R.M., Seixas, E., Seidman, J.S., Link, V.M., Sánchez, N.M., Mahú, I., Mendes, R., Gres, V., Kubasova, N., Morris, I., et al. (2017). Sympathetic neuron-associated macrophages contribute to obesity by importing and metabolizing norepinephrine. Nat. Med. *23*, 1309–1318.

Riffee, W.H., Ludden, T.M., Wilcox, R.E., and Gerald, M.C. (1978). Brain and plasma concentrations of amphetamine isomers in mice. J. Pharmacol. Exp. Ther. *206*, 586–594.

Ring, A.M., Manglik, A., Kruse, A.C., Enos, M.D., Weis, W.I., Garcia, K.C., and Kobilka, B.K. (2013). Adrenaline-activated structure of β2-adrenoceptor stabilized by an engineered nanobody. Nature *502*, 575–579.

Rothwell, N.J., and Stock, M.J. (1979). A role for brown adipose tissue in diet-induced thermogenesis. Nature *281*, 31–35.

Ruud, J., Steculorum, S.M., and Brüning, J.C. (2017). Neuronal control of peripheral insulin sensitivity and glucose metabolism. Nat. Commun. *8*, 15259.

Schneidman-Duhovny, D., Inbar, Y., Nussinov, R., and Wolfson, H.J. (2005). PatchDock and SymmDock: servers for rigid and symmetric docking. Nucleic Acids Res. *33*, W363-367.

Schwartz, J.H., Young, J.B., and Landsberg, L. (1983). Effect of dietary fat on sympathetic nervous system activity in the rat. J. Clin. Invest. *72*, 361–370.

She, P., Shiota, M., Shelton, K.D., Chalkley, R., Postic, C., and Magnuson, M.A. (2000). Phosphoenolpyruvate carboxykinase is necessary for the integration of hepatic energy metabolism. Mol. Cell. Biol. *20*, 6508–6517.

Spraul, M., Ravussin, E., Fontvieille, A.M., Rising, R., Larson, D.E., and Anderson, E.A. (1993). Reduced sympathetic nervous activity. A potential mechanism predisposing to body weight gain. J. Clin. Invest. *92*, 1730–1735.

Susulic, V.S., Frederich, R.C., Lawitts, J., Tozzo, E., Kahn, B.B., Harper, M.-E., Himms-Hagen, J., Flier, J.S., and Lowell, B.B. (1995). Targeted Disruption of the β 3 -Adrenergic Receptor Gene. J. Biol. Chem. *270*, 29483–29492.

Tschöp, M.H., Speakman, J.R., Arch, J.R.S., Auwerx, J., Brüning, J.C., Chan, L., Eckel, R.H., Farese, R.V., Galgani, J.E., Hambly, C., et al. (2012). A guide to analysis of mouse energy metabolism. Nat. Methods *9*, 57–63.

Ursino, M.G., Vasina, V., Raschi, E., Crema, F., and De Ponti, F. (2009). The beta3-adrenoceptor as a therapeutic target: current perspectives. Pharmacol. Res. *59*, 221–234.

Veronese, F.M. (2001). Peptide and protein PEGylation: a review of problems and solutions. Biomaterials *22*, 405–417.

Wang, C.C. (1924). Studies on the metabolism of obesity: III. The specific dynamic action of food. Arch. Intern. Med. *34*, 573.

Wang, J., Wolf, R.M., Caldwell, J.W., Kollman, P.A., and Case, D.A. (2004). Development and testing of a general amber force field. J. Comput. Chem. *25*, 1157–1174.

Warner, A., and Mittag, J. (2014). Brown fat and vascular heat dissipation: The new cautionary tail. Adipocyte *3*, 221–223.

Warner, A., Rahman, A., Solsjö, P., Gottschling, K., Davis, B., Vennström, B., Arner, A., and Mittag, J. (2013). Inappropriate heat dissipation ignites brown fat thermogenesis in mice with a mutant thyroid hormone receptor α1. Proc. Natl. Acad. Sci. U. S. A. *110*, 16241–16246.

Xiao, C., Goldgof, M., Gavrilova, O., and Reitman, M.L. (2015). Anti-obesity and metabolic efficacy of the β3-adrenergic agonist, CL316243, in mice at thermoneutrality compared to 22°C: Effect of Cl316243 at Thermoneutrality. Obesity *23*, 1450–1459.

Yang, Z., Fonović, M., Verhelst, S.H.L., Blum, G., and Bogyo, M. (2009). Evaluation of α,β-unsaturated ketone-based probes for papain-family cysteine proteases. Bioorg. Med. Chem. *17*, 1071–1078.

Zeng, W., Pirzgalska, R.M., Pereira, M.M.A., Kubasova, N., Barateiro, A., Seixas, E., Lu, Y.-H., Kozlova, A., Voss, H., Martins, G.G., et al. (2015). Sympathetic neuro-adipose connections mediate leptin-driven lipolysis. Cell *163*, 84–94.

**Supplementary Information:**

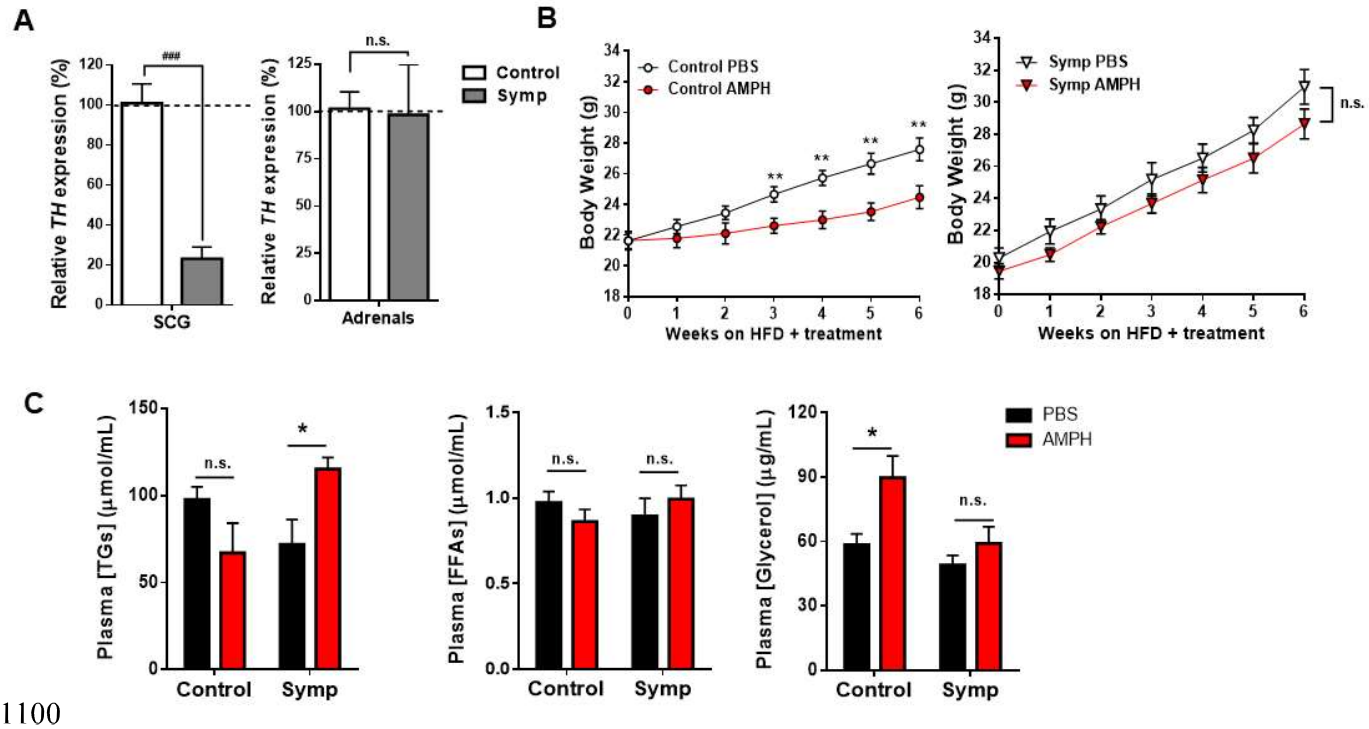


**Figure S1. The sympathomimetic action of AMPH is required for its anti-obesity effect and the elevation of lipolysis. A.** Levels of *TH* mRNA expression, in the superior cervical ganglia (SCG) and in the adrenal glands of Control and Symp mice, determined by qRT-PCR relative to the housekeeping gene GAPDH. B. Body weight of Control (left) and Symp (right) mice during 6 weeks of HFD exposure and PBS or AMPH treatment (dose: 120µmol/kg of BW, daily IP injections). **C.** Plasma Triglycerides (TGs), Free Fatty Acids (FFAs) and Glycerol content in HFD fed Control and Symp mice 2h post-injection without access to food. (*p<0.05; **p<0.01; ###p<0.001; n = 6-12. Statistics done using unpaired Student's *t*-test, with Holm-Sidak correction method. *PBS vs AMPH; #Control versus Symp). Data presented as mean ± S.E.M. Related to Figure 1.

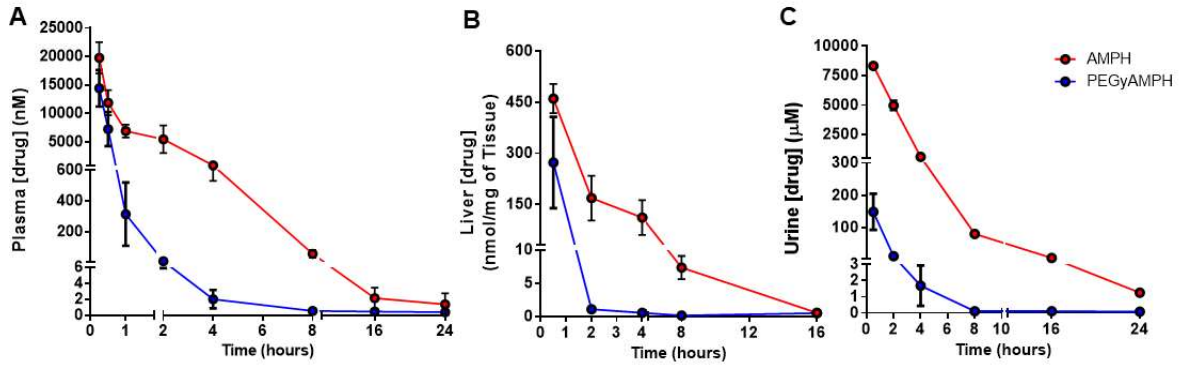


**D**

| Slc6a2 *(h)* ( [$^3$H]nisoxetine ) | | |
|---|---|---|
| **Compound I.D.** | **Concentration** | **% Control Uptake (Mean ± SEM)** |
| AMPH | 5.0E-05 M | 18.10 ± 2.10 |
| PEGyAMPH | 5.0E-05 M | 98.65 ± 2.05 |

**Figure S2. PEGylation of AMPH reduces excretion and alters its pharmacological properties. A.** Time course of the plasma concentration of AMPH or PEGyAMPH, post IV injection (dose: 120 µmol/kg of BW), assessed by mass spectrometry. **B-C.** Time course of the concentration of AMPH or PEGyAMPH, in the liver (**B**) and in the urine (**C**) of C57BL/6. **D.** Summary of *in vitro* radioligand ([$^3$H]nisoxetine) competition assays with AMPH and with PEGyAMPH (0,5µM) for the binding to Slc6a2. Data presented as mean ± S.E.M. Related to Figure 2.

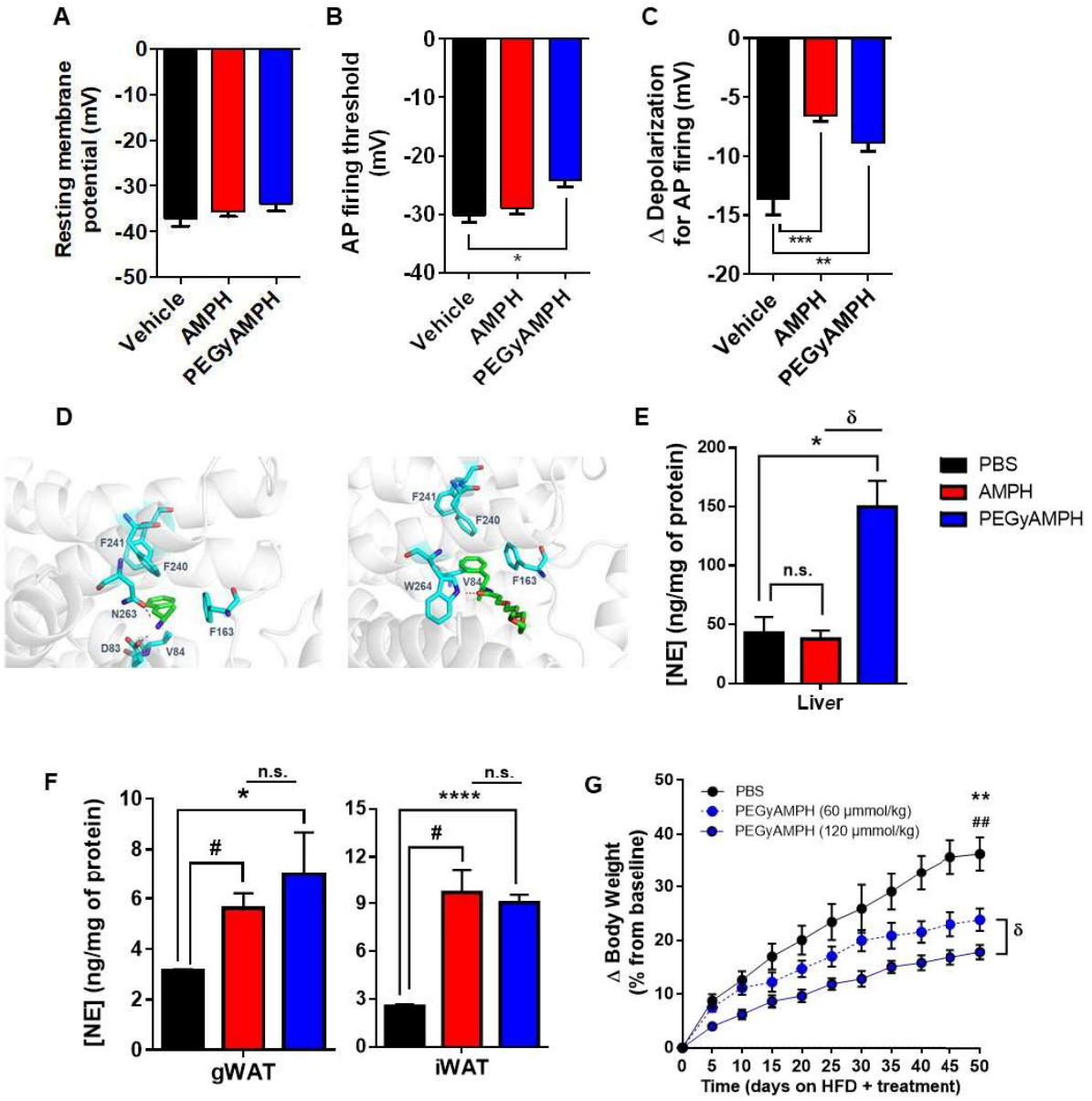


**Figure S3. PEGyAMPH facilitates SNS activation and increases NE availability in target tissues.** **A.** Resting membrane potential**. B.** AP firing threshold and **C.** Δ depolarization for AP firing of Vehicle, AMPH and PEGyAMPH-treated neurons (*p<0.05; **p<0.01; *** p<0.001; n = 8; Statistics done using one-way ANOVA followed by Bonferroni correction). **D.** 3D structure of $\beta_1$-adrenoceptor in complex with AMPH and PEGyAMPH. Left: Minimized structure calculated by Molecular Mechanics (MM) for $\beta_1$-adrenoceptor/AMP complex, showing the most relevant interactions between AMP and the receptor. Right: Minimized structure calculated by MM for $\beta_1$-adrenoceptor/PEGyAMP complex, showing the most relevant interactions ligand-receptor. The receptor is represented as white ribbons and the carbon atoms of the residues of the receptor that are interacting directly with the ligands are in blue. The carbon atoms of the ligands are in green. and in the **E.** NE content in the Liver and **F.** NE content in gonadal and inguinal White Adipose Tissue (gWAT and iWAT, respectively) of C57BL/6 mice 3-4h post-injection, with PBS, AMPH and PEGyAMPH (dose: 120 µmol/kg of BW for both drugs, IP). **G.** ΔBW of C57BL/6 mice exposed to HFD and treatment with PBS or two different doses of PEGyAMPH (0,06 and 120 µmol/kg of BW, daily IP injections). (*,#,$^{\delta}$p<0.05; **p<0.01; ###p<0.001; ****p<0.0001, n = 8-10. Statistics done using unpaired Student's *t*-test,

with Holm-Sidak correction. *PBS versus PEGyAMPH; #PBS versus AMPH; δAMPH versus PEGyAMPH.)
Data presented as mean ± S.E.M. Related to Figure 3.

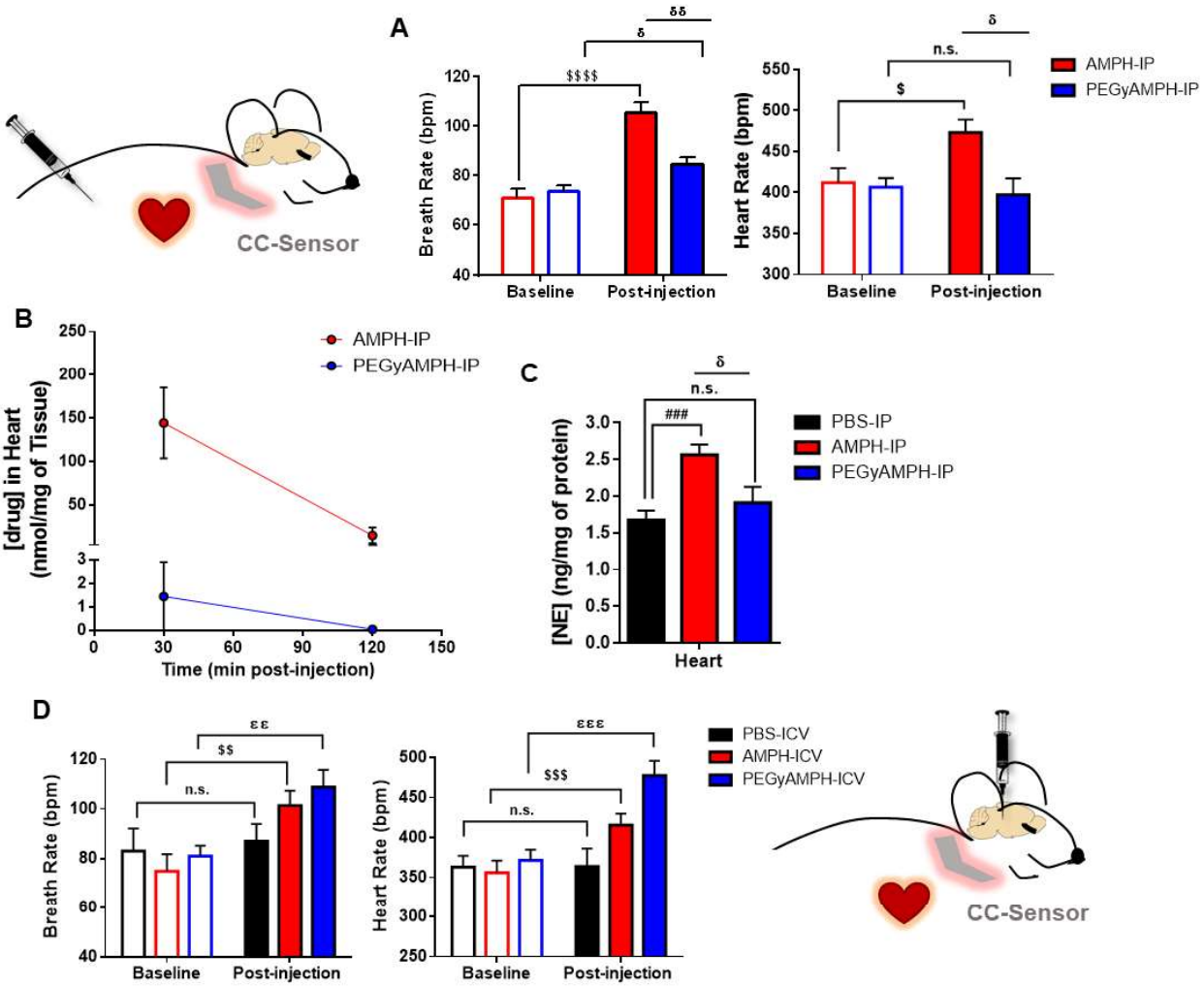


**Figure S4. PEGyAMPH, unlike AMPH, does not affect cardiovascular function. A.** Breath Rate and Heart Rate measured under anaesthesia (1-2% isoflurane) using a CC-Sensor for pulse-oximetry, before and 30-45min post IP injection with PEGyAMPH or AMPH (dose: 120 µmol/kg of BW for both drugs). **B.** Drug concentration in the Heart of C57BL/6 mice injected post IP injection (dose: 120 µmol/kg of BW for both drugs), assessed by mass spectrometry. **C**. Heart NE content measured 30 min post IP injection. **D.** Breath Rate and Heart Rate measured before and 15-30min post ICV injection with either PBS, AMPH or PEGyAMPH (bolus of 60nmol, per animal) of C57BL/6 mice. ($^{\#}$,$^{\$}$,$^{\delta}$p<0.05; $^{\$\$}$,$^{\delta\delta}$,$^{\varepsilon\varepsilon}$p<0.01, $^{\$\$\$}$,$^{\varepsilon\varepsilon\varepsilon}$p<0.001, $^{\#\#\#\#}$,$^{\$\$\$\$}$p<0.0001; n = 8-12. Statistics done using unpaired Student's *t*-test, with Holm-Sidak correction method. $^{\#}$PBS vs AMPH; $^{\delta}$AMPH versus PEGyAMPH; $^{\$}$Baseline versus AMPH; $^{\varepsilon}$Baseline versus PEGyAMPH;). Data presented as mean ± S.E.M. Related to Figure 4.

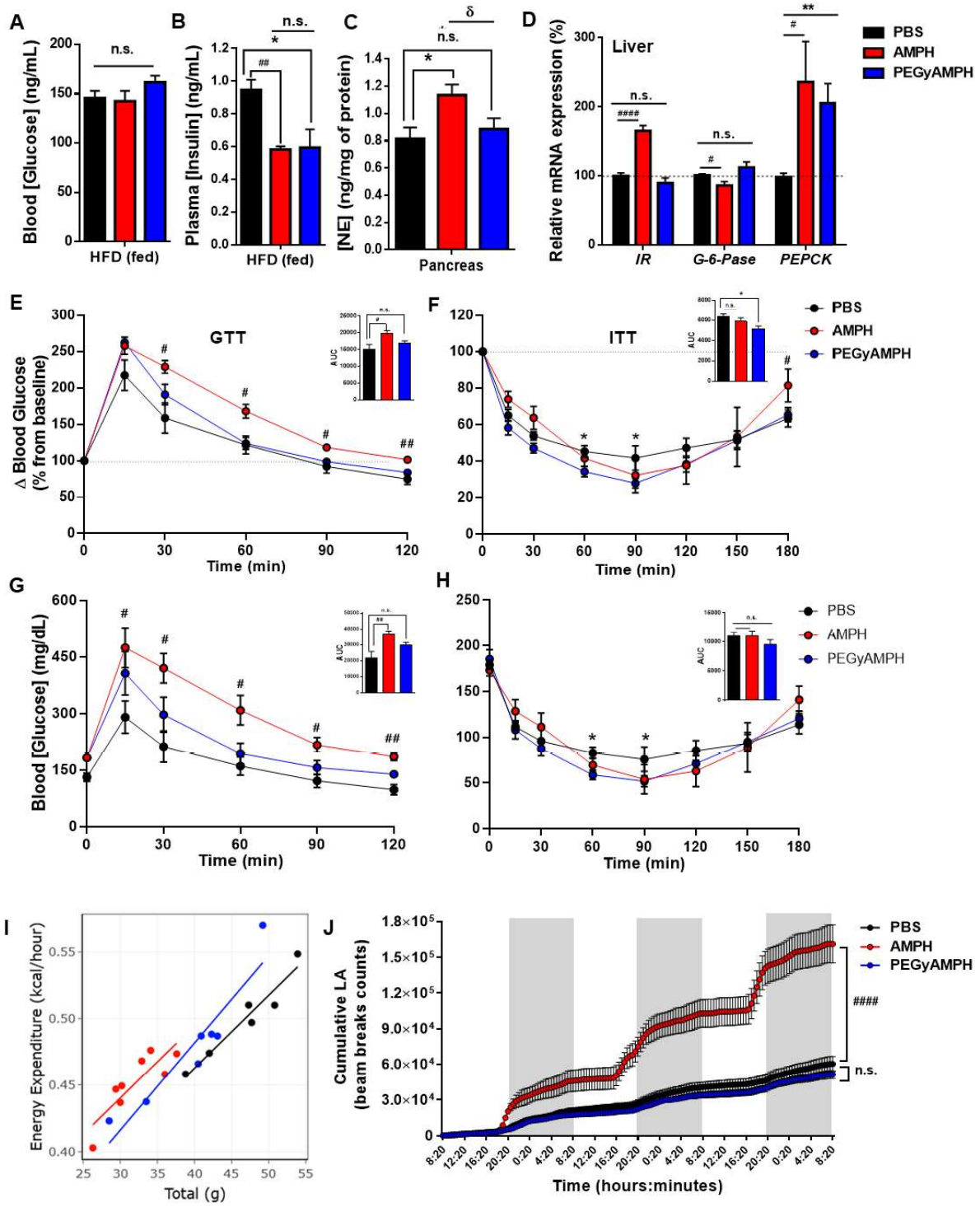


**Figure S5. PEGyAMPH improves insulin sensitivity by increasing EE, without affecting Locomotor Activity (LA). A.** Blood Glucose and **B.** Plasma Insulin levels, **C.** Pancreatic NE content. **D.** Liver gene expression levels of *IR* and gluconeogenic genes Glucose 6-phosphatase (*G-6-Pase*) and Phosphoenolpyruvate carboxykinase (*PEPCK*) determined by qRT-PCR relative to housekeeping gene *GAPDH,* of fed mice 2 h post injection and without access to food, after 10 weeks of HFD exposure and respective treatment. (**E-H**). Metabolic and behavioural test were performed during the fourth and fifth

weeks of HFD exposure and respective treatment **E** and **G.** Intraperitoneal Glucose Tolerance Test (GTT, glucose bolus of 2g/kg of BW) performed 6h post injection with PBS, AMPH or PEGyAMPH without access to food, and the respective AUC for 120min blood glucose levels. **F** and **H.** Insulin Tolerance Test (ITT, insulin bolus of 0.9U/kg of BW) performed 2h post injection with PBS, AMPH or PEGyAMPH (dose: 120 µmol/kg of BW for both drugs) without access to food, and the respective AUC for 180min blood glucose levels**. I.** Relation between the average EE and total body mass. **J.** Cumulative Locomotor Activity (LA) measured for 72h, represented in beam breaks counts. (*,$^{\#}$;$^{\delta}$p<0.05, **,$^{\#\#}$p<0.01; $^{\#\#\#\#}$p<0.0001, n = 8-15. Statistics done using unpaired Student's t-test, with Holm-Sidak correction method. *PBS versus PEGyAMPH; $^{\#}$PBS versus AMPH; $^{\delta}$PEGyAMPH versus AMPH.) Data presented as mean ± S.E.M. Related to Figure 5.

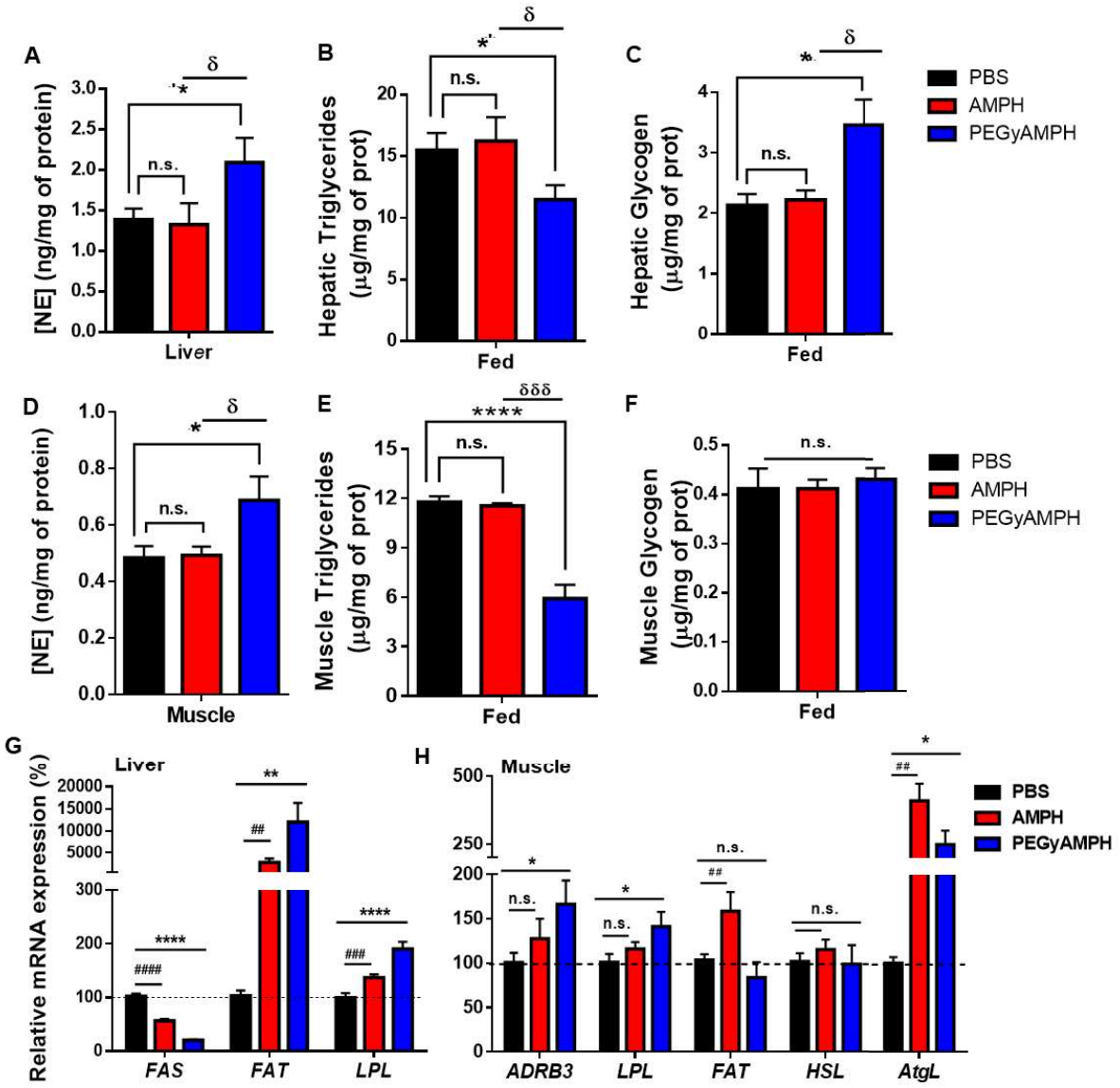


**Figure S6. PEGyAMPH elevates peripheral lipid utilization during DIO. (A-C** and **G)** Liver and **(D-F** and **H)** Muscle measurements from fed C57BL/6 mice after 10 weeks of HFD exposure and chronic treatment with PBS, AMPH or PEGyAMPH. **A.** NE, **B.** TGs and **C.** Glycogen content in the liver and **D.** NE, **E.** TGs and **F.** Glycogen content in muscle, all values were normalized to total protein levels. **G.** Liver mRNA levels of Fatty Acid Transporter (*FAT*), Lipoprotein Lipase (*LPL*) and Fatty Acid Synthase (*FAS*) determined by qRT-PCR relative to housekeeping gene *GAPDH*. **H.** Muscle mRNA levels of *ADRB3*, *LPL, FAT*, *HSL* and *AtgL* determined by qRT-PCR relative to housekeeping gene *GAPDH*. (*,$^{\delta}$p<0.05; **,$^{\#\#}$p<0.01; $^{\#\#\#}$;$^{\delta\delta\delta}$p<0.001; ****,$^{\#\#\#\#}$p<0.0001; n = 12. Statistics done using unpaired Student's *t*-test, with Holm-Sidak correction. *PBS versuss PEGyAMPH; $^{\#}$PBS versus AMPH; $^{\delta}$PEGyAMPH versus AMPH.) Data presented as mean ± S.E.M. Related to Figure 6.

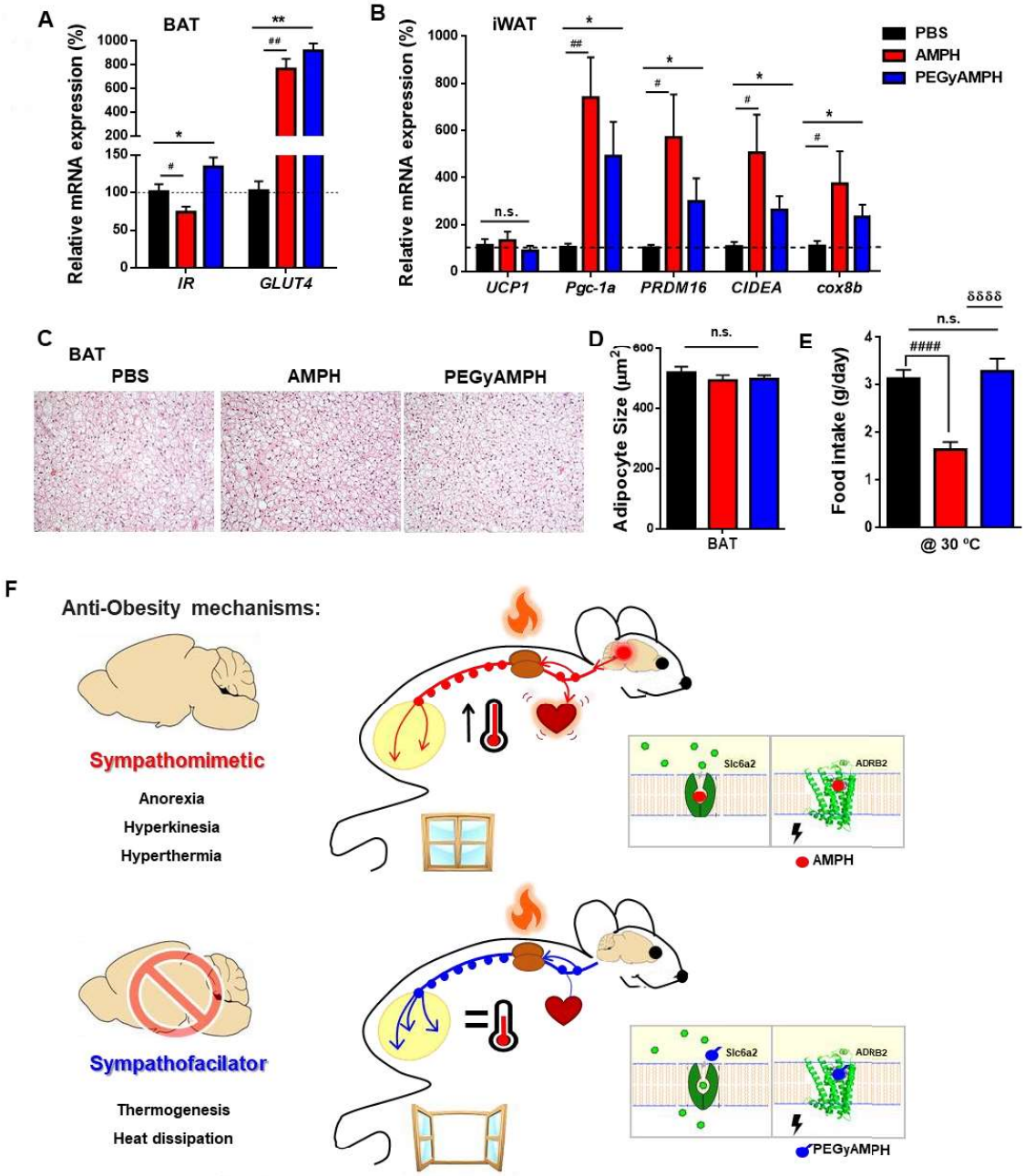


**Figure S7. PEGyAMPH increases Thermogenesis during DIO. A.** BAT mRNA levels of the Insulin Receptor (*IR*) and of the Glucose Transporter type 4 isoform (*GLUT4*) and **B.** iWAT mRNA levels of thermogenic genes, gene expression was determined by determined by qRT-PCR, relative to housekeeping gene *Arbp0*. **C.** Representative Histologic Slices of BAT stained with H&E and **D.** Quantification of BAT Adipocyte Size of C57BL/6 mice after 10 weeks of HFD exposure and treatment with PBS, AMPH or PEGyAMPH (dose: 120 µmol/kg of BW for both drugs, daily IP injections). **E.** Daily Food Intake of C57BL/6 mice mice exposed to HFD and treatment with PBS, AMPH or PEGyAMPH (dose: 120 µmol/kg of BW for both drugs, daily IP injections) under thermoneutral housing conditions. **F.** Schematic summary of the mechanism of action for anti-obesity treatment of the two sympathomimetics used in this study. (*,$^{\#}$p<0.05; **,$^{\#\#}$p<0.01, $^{\#\#\#\#}$,$^{\delta\delta\delta\delta}$p<0.0001 n = 5-12. Statistics done using unpaired Student's *t*-test, with Holm-Sidak correction. *PBS versus PEGyAMPH; $^{\#}$PBS versus AMPH, $^{\delta}$AMPH versus PEGyAMPH.) Data presented as mean ± S.E.M. Related to Figure 7.

**Table S1. List of qPCR primers:**

| Primer | Sequence |
|---|---|
| *Arbp0* Fwd | 5´ CTTTGGGCATCACCACGAA 3´ |
| *Arbp0* Rev | 5´ GCTGGCTCCCACCTTGTCT 3´ |
| *GAPDH* Fwd | 5´ AACTTTGGCATTGTGGAAGG 3´ |
| *GAPDH* Rev | 5´ ACACATTGGGGGTAGGAACA 3´ |
| *IR* Fwd | 5’ ATGGGCTTCGGGAGAGGAT 3’ |
| *IR* Rev | 5’ GGATGTCCATACCAGGGAC 3’ |
| *GLUT4* Fwd | 5’ TTGGCTCCCTTCAGTTTGG 3’ |
| *GLUT4* Rev | 5’ CTACCCAGCCACGTTGCAT 3’ |
| *G-6-Pase* Fwd | 5’ CGACTCGCTATCTCCAAGTGA 3’ |
| *G-6-Pase* Rev | 5’ GTTGAACCAGTCTCCGACCA 3’ |
| *PEPCK* Fwd | 5’ CTGCATAACGGTCTGGACTTC 3’ |
| *PEPCK* Rev | 5’ CAGCAACTGCCCGTACTCC 3’ |
| *ADRB3* Fwd | 5’ ATCATGAGCCAGTGGTGGCGTGTAG 3’ |
| *ADRB3* Rev | 5’ GCGATGAAAACTCCGCTGGGAACTA 3’ |
| *AtgL* Fwd | 5’ TGGTTCAGTAGGCCATTCCT 3’ |
| *AtgL* Rev | 5’ CACTTTAGCTCCAADDATGA 3’ |
| *HSL* Fwd | 5’ TGCTCTTCTTCGAGGGTGAT 3’ |
| *HSL* Rev | 5’ TCTCGTTGCGTTTGTAGTGC 3’ |
| *LPL* Fwd | 5’ CAGCTGGGCCTAACTTTGAG 3’ |
| *LPL* Rev | 5’ CCTCTCTGCAATCACACGAA 3’ |
| *FAS* Fwd | 5’ CCCTTGATGAAGAGGGATCA 3’ |
| *FAS* Rev | 5’ ACTCCACAGGTGGGAACAAG 3’ |
| *FAT/CD36* Fwd | 5′ TGGCCTTACTTGGGATTGG 3′ |
| *FAT/CD36* Rev | 5′ CCAGTGTATATGTAGGCTCATCCA 3′ |
| *Ucp1* Fwd | 5’ ACTGCCACACCTCCAGTCATT 3’ |
| *Ucp1* Rev | 5’ CTTTGCCTCACTCAGGATTGG 3’ |
| *Pgc1a* Fwd | 5’ CCCTGCCATTGTTAAGAC 3’ |
| *Pgc1a* Rev | 5’ TGCTGCTGTTCCTGTTTTC 3’ |
| *PRDM16* Fwd | 5’ CAGCACGGTGAAGCCATT 3’ |
| *PRDM16* Rev | 5’ GCGTGCATCCGCTTGTG 3’ |
| *CIDEA* Fwd | 5’ TGCTCTTCTGTATCGCCCAGT 3’ |
| *CIDEA* Rev | 5’ GCCGTGTTAAGGAATCTGCTG 3’ |
| *cox8b* Fwd | 5’ GAACCATGAAGCCAACGACT 3’ |
| *cox8b* Rev | 5’ GCGAAGTTCACAGTGGTTCC 3’ |

1191